Seasonal Near-Surface Dynamics and Thermodynamics of the Indian Ocean and Indonesian Throughflow in a Global Ocean General Circulation Model

A. SCHILLER, J. S. GODFREY, P. C. MCINTOSH, G. MEYERS, AND S. E. WIJFFELS

CSIRO Division of Marine Research, Hobart, Tasmania, Australia

(Manuscript received 12 September 1997, in final form 24 February 1998)

ABSTRACT

The near-surface dynamics and thermodynamics of the Indian Ocean are examined in a global ocean general circulation model (OGCM) with enhanced tropical resolution. The model uses a Seager-type heat flux formulation (weak relaxation toward a fixed SST, flux-corrected toward seasonal observed values). Resulting seasonal patterns of surface heat flux, mixed layer depth, and surface steric height all compare quite well with observations in the Indian Ocean, away from western boundaries. Distribution of flow in the mean Indonesian Throughflow is quite well simulated in the top 700 m. The model Indonesian throughflow transports, on average, 16.3×10^6 m^3 s^{-1} from the Pacific to the Indian Ocean, and its magnitude is fairly well predicted seasonally by the instantaneous Sverdrup version of the ''Island Rule.'' Model geostrophic transports relative to 700 m are substantially smaller, with a different seasonal cycle. Observed geostrophic transports are smaller than those in the model, though the model reproduces the seasonal cycle well. The annual mean heat transport through the Indonesian Throughflow region (about 1.15×10^{15} W) represents a heat sink for the Pacific Ocean and is an important heat source for the Indian Ocean. The authors have introduced an empirically based representation of tidal mixing in the Indonesian region: it causes water mass transformation through the Indonesian seas qualitatively like that observed and improves the realism of the surface heat fluxes. It also affects both the Indian and Pacific Oceans and causes extensive subsurface temperature and salinity changes in the former (i.e., cooling of the mixed layer, warming of the upper thermocline).

1. Introduction

Several studies (e.g., Neelin et al. 1992; Stockdale et al. 1993; Mechoso et al. 1995) have recently indicated that much of the climatic variability on seasonal to interannual timescales results from interactions of the World Ocean and the atmosphere. Due to its large heat capacity, the ocean plays a crucial role in coupled models since it modulates the variations of the climate system. Whereas a lot of research has been done to understand the dynamics of the El Niño–Southern Oscillation as a major feature evolving from the Pacific Ocean, comparably little has been spent to understand the complexity of the Indian Ocean circulation system and the way it transports heat and freshwater (e.g., Wacongne and Pacanowski 1996; Schmitz 1996b; Lee and Marotzke 1997). We describe a model of the World Ocean's general circulation, designed ultimately to realistically simulate interannual variations of sea surface temperature (SST) in low latitudes, including the Indian Ocean. As a prerequisite for reasonable simulations of SST variations on interannual and longer timescales, one has to have confidence in the model's simulation of the seasonal cycle. Thus, much of the emphasis of this paper is on the seasonal behavior of the upper ocean, which controls SST and its anomalies in the Tropics. This subject has been dealt with in some earlier papers (e.g., McCreary et al. 1993; Wacongne and Pacanowski 1996). However, model simulation of SST anomalies (and mean seasonal mixed layer depths) depend strongly on the choice of surface heat flux boundary conditions. We have chosen this condition with some care, to get an observationally based heat flux product that has the potential to vary interannually. Since our emphasis is on understanding the seasonal cycle of SST—and especially its anomalies—we revisit some topics dealt with in earlier papers.

A second focus of this paper is on the Indian Ocean and the Indonesian Throughflow (ITF). Particular attention is given to the ITF area because it allows warm Pacific water to flow into the Indian Ocean and, thus, is expected to form an important part of the global circulation system (e.g., Schmitz 1996a,b). Variations of the throughflow certainly affect SST in the Indonesian region, and SST fluctuations in the ITF region have been shown to correlate with rainfall over Indonesia and Australia (Nicholls 1989; Drosdowsky 1993).

Strong tidal flow in the Indonesian region enhances the mixing of deep and surface waters, as water flows

Corresponding author address: Dr. Andreas Schiller, CSIRO Division of Marine Research, GPO Box 1538, Hobart, Tasmania 7001, Australia.
E-mail: schiller@marine.csiro.au

from the Pacific to the Indian Ocean (Ffield and Gordon 1992) and thus modifies SST significantly. Our ocean model has a parameterization of tidal mixing based on observations (Ffield and Gordon 1996); this has not been studied before in a global ocean circulation model.

The paper continues with a short description of the model configuration, emphasizing the parameterization of heat fluxes. In the following sections we assess three important features that influence interannual variability in the Indian Ocean. Section 3 assesses the seasonal simulation of surface heat fluxes and upper-ocean dynamics in the Indian Ocean by comparison with observations. In section 4, we discuss the mass and heat transports through the ITF and compare the model results to observational estimates. Section 5 investigates the impact of simulated tidal mixing on the Indian Ocean. We conclude the paper with a summary and discussion of the results. The anticipated reasonable performance of the model under seasonal forcing conditions forms the basis for an investigation of the interannual dynamics in a second paper (Schiller et al. 1998, submitted to *J. Phys. Oceanogr.*).

2. Model description

a. Model configuration

1) GRID AND TOPOGRAPHY

The model used in this study is a recent version of the GFDL (Geophysical Fluid Dynamics Laboratory) primitive equations Modular Ocean Model [MOM2; (Pacanowski 1995)]. The global model has a tropically enhanced resolution to give a realistic simulation of low-latitude ocean physics. The grid spacing is 2° in the zonal direction. The meridional spacing is 0.5° within 8° of the equator, increasing gradually to 5.85° near the poles. There are 82 grid points from south to north and 182 grid points from west to east. The model has 25 levels in the vertical, with 12 levels in the top 185 m. The maximum depth is 5000 m. The level thicknesses range from 15 m near the surface to almost 1000 m near the bottom (Schiller et al. 1997).

The bathymetry of the model represents a smoothed approximation to the high-resolution dataset of Gates and Nelson (1975). To simulate the ITF we modified the model's topography in that area, allowing for a transport of water masses through Lombok Strait and the Timor Sea. Because islands are computationally expensive in this version of the GFDL model, only the Philippines, Kalimantan, Celebes, the Lombok–Flores Islands, Australia (combined with New Guinea and Tasmania), New Zealand, and Antarctica are modeled explicitly (Fig. 1). There is no Bering, Torres, or Bass Strait. Drake Passage was artificially widened to aid throughflow of the Antarctic Circumpolar Current.

The flows of the Red Sea into the Indian Ocean and the Mediterranean Sea into the Atlantic Ocean significantly change the water-mass structures of these oceans. Because the Red and Mediterranean Seas are not included in the model, their effects are simulated by restoring temperature and salinity to observed values (Levitus 1982) at their points of exchange with the Indian and Atlantic Ocean, respectively, over the whole water column. To maintain the characteristic water mass properties in the Indian and Atlantic Ocean, a damping timescale of 7 days for the surface was chosen, which gradually increases to 30 days in the deep ocean. This timescale is much shorter than used conventionally (a few weeks at the surface and a few months for the abyssal ocean) because the important hydrological signal of the inflows vanishes if a traditional timescale is used.

Due to the strong changes in grid sizes in the model (enhanced tropical grid and coarse resolution close to the poles) and in order to guarantee numerical stability, the zonal and meridional viscosities are dependent on latitude. The modifications are similar to those Power et al. (1995) applied to an earlier version of the model. The meridional viscosity is set to 2.0×10^3 m^2 s^{-1} near the equator, increasing to over 3.1×10^5 m^2 s^{-1} at high latitudes, while the zonal viscosity is 2.0×10^4 m^2 s^{-1} near the equator, also increasing to over 3.1×10^5 m^2 s^{-1} at high latitudes. The horizontal diffusivity is set to 4.0×10^3 m^2 s^{-1} everywhere.

To assure stability of the numerical integration, a time step of 900 seconds is used for all prognostic variables (i.e., for tracers, and internal and external mode velocities).

2) MIXED LAYER PARAMETERIZATION

Recent improvements to numerical vertical mixing schemes offer a variety of alternatives with reasonable simulations of observed mixed layer dynamics (e.g., Blanke et al. 1997; Chen et al. 1994b; Large et al. 1994). We decided to adopt the approach of Chen et al. (1994a), where vertical mixing and vertical friction are parameterized by a one-dimensional mixing scheme. It was implemented for level models by Power et al. (1995). Strong mixing is assumed to occur within a bulk mixed layer, as in the Niiler and Kraus (1977) model. Below the mixed layer, internal mixing is parameterized by a gradient Richardson-number-dependent mixing based on observations by Peters et al. (1988). Their observations show less mixing at higher Richardson numbers than the more widely used Pacanowski and Philander (1981) mixing scheme and particularly improves the model performance at lower latitudes (e.g., lower upwelling velocities along the equator; less prominent SST cold tongue in the eastern Pacific: both improving agreement with observations). The hybrid structure of this mixing scheme allows its application to high latitudes (where mixing is strongly influenced through the W^3 term by the high wind speeds, and thus the Niiler–Kraus part dominates); and also to the equatorial ocean (where vertical mixing is predominantly determined by large

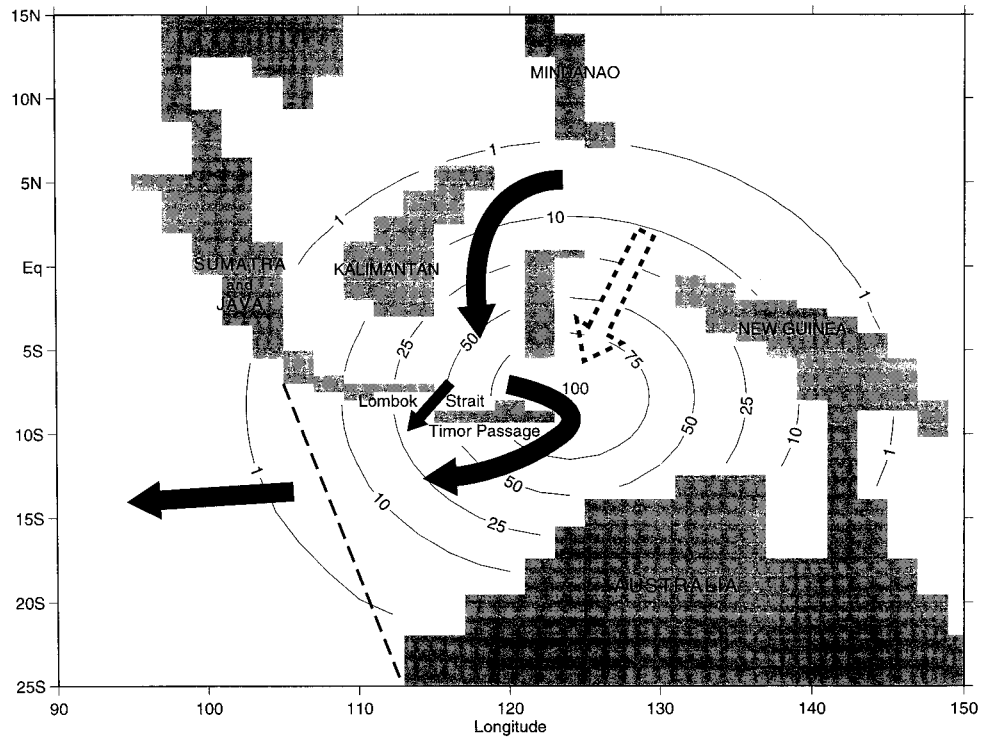

FIG. 1. Surface topography of the modeled Indonesian archipelago. The two gaps that allow Pacific water masses to enter the Indian Ocean are Lombok Strait and Timor Passage (as indicated by arrows). The isolines denote additional diffusion/viscosity that has been used to simulate tidal mixing. Values are in percent relative to its maximum value of 2×10^{-4} m^2 s^{-1} in the center of the Banda Sea. The dashed line between Java and West Australia indicates the WOCE XBT section IX1. See text for further details.

vertical current shears, and thus the gradient Richardson number part dominates). The maximum values for viscosity and diffusivity in the mixed layer are set to 266.0 $\times 10^{-4}$ m^2 s^{-1} and 199.0 $\times 10^{-4}$ m^2 s^{-1}, respectively. The background values (i.e., the smallest possible values for viscosity and diffusivity) are set to 0.2 $\times 10^{-4}$ m^2 s^{-1} and 0.01 $\times 10^{-4}$ m^2 s^{-1}, respectively. For a detailed discussion of the Chen et al. (1994b) mixed layer model in this form and tests with observed data, we refer to the report of Godfrey and Schiller (1997).

3) INDONESIAN THROUGHFLOW

Particular attention in the model is given to the ITF area because it allows warm Pacific water to flow into the Indian Ocean and because SST and energetic heat exchanges in this region have been shown to correlate with Australia's rainfall (Nicholls 1989).

As water flows from the Pacific to the Indian Ocean, the tidally induced vertical mixing in the Indonesian archipelago causes enhanced mixing of deep and surface waters and therefore is able to change the water-mass structure of the Indian Ocean significantly (Ffield and Gordon 1992; Hatayama et al. 1996). A recent analysis by Ffield and Gordon (1996, their Figs. 11a and 11b) suggests that the center of the tidal mixing effect on SST is the Banda Sea. To simulate this observed feature, the vertical mixing coefficients for diffusion and momentum were increased within the whole water column in the Indonesian area. This was done by defining a spatial exponential function similar to the sum of Ffield and Gordon's figures, which describes the spatial shape of the additional vertical mixing. The maximum value of the additional ''tidal mixing'' in the Banda Sea is 2 $\times 10^{-4}$ m^2 s^{-1}. This value gradually decreases as the distance from the Banda Sea increases (Fig. 1). This mixing is independent of time (i.e., no attempt was made to resolve the timescales associated with its physical origin): the only concern is its larger timescale effects on water mass properties, especially SST. In section 5 we show that this parameterization of tidal mixing in the Indonesian region leads to improved SST and heat flux patterns there.

The most recent survey of measurements of the transport of the Indonesian Throughflow indicates a current that is highly variable, with a mean geostrophic transport relative to 700 m of 5–10 Sv (Sv $\equiv 10^6$ m^3 s^{-1}) (Wijffels et al. 1996). Uncertainties in the total transport arise from a lack of measurements of deep shear (the reference level used in geostrophic calculations) and relatively little data on salinity variation. Routine XBT measurements over 13 years indicate that most of the throughflow enters the region through Makassar Strait

east of Kalimantan (Fig. 1) then flows eastward across the Flores and Banda Seas to enter the Indian Ocean near Timor Island through Ombai Strait and Timor Passage (Cresswell et al. 1993; Meyers et al. 1995). Nevertheless, direct current-meter measurements over one year indicate that 2 Sv entered the Indian Ocean through Lombok Strait, flowing directly southward from Makassar Strait (Murray and Arief 1988). Although the measurements are not definitive, we have assumed that 80% of the model's flow enters the Indian Ocean near Timor. A high cross-strait meridional eddy viscosity was built into the model's Lombok Strait to simulate the observed bifurcation of transports. By trial and error, the meridional eddy viscosity in Lombok Strait was increased to eight times the dissipation elsewhere at this latitude. The resulting throughflow closely approximates the target defined above and will be discussed in section 5. The model's sill depths in Lombok Strait and the Timor Passage are 613 and 2342 m, respectively.

b. Surface flux formulations

Interannually varying estimates of the various fluxes for the period 1985–90 have been averaged to create the seasonal forcing climatologies for this paper (the only period for which satellite-based shortwave radiation estimates were available).

1) MOMENTUM FLUXES

The monthly mean Florida State University (FSU) ''pseudostresses'' for 1985–90 for the Indian and Pacific Oceans were used (Legler et al. 1989; Stricherz et al. 1992) with a constant bulk transfer coefficient, C_D, of 0.0015. Monthly mean wind stresses have been constructed from these data. The FSU winds are only available from 30°N to 30°S: poleward of these latitudes, the data have been blended into Hellerman and Rosenstein (1983) seasonal mean wind stresses. To avoid inhomogenities in the transition regions, the data were blended over three grid points, covering 6° of longitude and approximately 10° of latitude. Inspection of the wind stress curl, Ekman pumping, and Ekman transport reveals a smooth variation of these properties in the blending zones (not shown).

2) FRESHWATER FLUXES

The surface layer of the model (15 m thick) has been relaxed to observed seasonal mean surface salinity, with a time constant of 17 days. The surface salinities were taken from Levitus (1982).

3) HEAT FLUXES

It has been appreciated recently, starting with Seager et al. (1988), that if air temperature T_a and relative humidity RH are allowed to respond realistically to changes in SST [e.g., by keeping (SST $-$ T_a) and RH constant], then the effective ''damping coefficient,'' or rate of change of net surface heat flux $\partial Q_{\text{tot}}/\partial T_s$ with surface temperature, is remarkably low—about 15 W m^{-2}/°C in the Tropics. This is so low that a constant 30 W m^{-2} error in surface heat flux [which is probably present in the shortwave radiation product alone, e.g., Chen et al. (1994a)] will generate an unacceptably large, constant 2°C offset in SST. Such errors would be unacceptable in a model designed for coupling to an atmospheric model for climate prediction work; so in testing it we need to adopt the same strategy used in many coupled models—i.e., to apply mean seasonal ''flux corrections.'' This consideration has guided our choice of a heat flux formulation. A more detailed discussion, and a review of relevant recent literature (e.g., Chen et al. 1994a; Seager and Blumenthal 1994; Kleeman and Power 1995; Rahmstorf and Willebrand 1995), is given in Godfrey and Schiller (1997). Because of the importance of this topic, we devote some space here to our choice of surface heat flux boundary condition.

We chose the following formula for the net heat flux Q_{tot} (Seager et al. 1988; Chen et al. 1994a):

$$Q_{\text{tot}} = R_s - \rho_a C_E L_v W(0.98 - \delta) q_{\text{sat}}(T_s) - \alpha'(T_s - T^*) - Q_{\text{correct}}. \quad (1)$$

Looking at the four terms on the right-hand side of Eq. (1), the first term, R_s, is the ISCCP ''bulk'' estimate of net downward shortwave radiation (Li 1995). The second term corresponds to latent heat exchange, where ρ_a, C_E, and L_v are the air density, bulk transfer coefficient, and latent heat of vaporization, respectively; W is an estimate of wind speed: $W^2 = |U_\tau| + W_0^2$, where $|U_\tau|$ is the magnitude of the monthly mean FSU wind pseudostress estimate and W_0 is a ''gustiness estimate'' with $W_0 = 3$ m s^{-1}; $q_{\text{sat}}(T_s)$ is the saturated water vapor pressure over freshwater at the surface temperature T_s. The factor of 0.98 accounts for ocean salinity. The ratio δ of the specific humidities between the marine–atmosphere boundary layer and the saturated value at the ocean's surface has been calculated as a function of season and position from the COADS climatology (da Silva et al. 1994).

The third term represents the sum of sensible heat exchange and net longwave radiation, with $\alpha' = 1.5$ W m^{-2}/°C. According to the Oberhuber (1988) climatology, this sum roughly equals 55 W m^{-2} over the tropical Pacific and Indian Oceans. We have chosen $T^* = -8$°C. At typical tropical SST of 28°C gives $\alpha'(T_s - T^*) =$ 54 W m^{-2}. Given reliable observed shortwave radiation, the formula (1) is accurate within the errors of order 20 W m^{-2} or better in these estimates, as demonstrated by Godfrey and Schiller (1997) in a test over the 4-month-long accurate flux dataset obtained during TOGA COARE.

The last term, Q_{correct}, is a ''flux correction,'' which accounts for the small SST damping rate, $\partial Q_{\text{tot}}/\partial T_s$, of

about 15 W m^{-2}/°C (for typical wind speeds using the constants above).

In Eq. (1) Q_{tot} is further separated into

$$Q_{tot} = Q_{surface} + Q_{penetrating}. \quad (2)$$

The latter term is assumed to fall off exponentially with depth, according to the formula

$$Q_{penetrating} = R_s 0.4 e^{-kz}, \quad (3)$$

which approximates the formula of Paulson and Simpson (1977). Their formulation accounts for the different attenuation lengths of the infrared and penetrative wavelengths of the solar spectrum. Infrared wavelengths are absorbed within the uppermost few meters of the ocean. Because the top model level is 15 m thick, the attenuation lengths are combined as in Eq. (3). The decay rate k varies with position according to empirical estimates of turbidity (Simonot and Le Treut 1986). Unfortunately, this data precludes the seasonal resolution of the solar shortwave penetration in the ocean.

4) Flux corrections

The flux correction $Q_{correct}$ was obtained for the period 1985–90 by

1) estimating the mean seasonal cycle of R_s from the ISCCP data;
2) estimating the mean seasonal cycle of SST, $T_{Reyn\text{-}seas}$, from the Reynolds (Reynolds 1988; Reynolds and Smith 1994) data;
3) estimating the mean seasonal cycle of the wind speed W from the FSU data;
4) estimating the mean seasonal cycle of the ratio of specific humidities δ from the COADS climatology.

The model integrations were then started from a state of rest with the hydrography (Levitus 1982) interpolated to the model grid. During the 20-yr spinup phase of the model, Eq. (1) was used, but with T_s replaced by the temperature of the upper model level, T_{model}. Here $Q_{correct}$ was replaced by

$$Q_{correct} = \lambda(T_{model} - T_{Reyn\text{-}seas}) \quad (4)$$

with an artificially large damping coefficient λ of 100 W m^{-2}/°C. With this choice, typical maximum flux errors of up to 50 W m^{-2} and SST errors of up to 0.5°C will contribute about equally. During the last year of the spinup, the monthly averages of $\lambda(T_{model} - T_{Reyn\text{-}seas})$ were stored for use in Eq. (1) in the seasonally and interannually (Schiller et al. 1998) forced experiments.

The seasonally forced experiments should be almost insensitive to the imposed heat flux correction (i.e., the restoring term from year 20 of the spinup run should not be significantly different from an assumed restoring term at year 6 of the experiment). However, the concept of modeling interannual variability relies heavily on the assumption that the seasonal heat flux correction improves the ''background'' heat fluxes without affecting the interannual components. Unfortunately, reliable surface forcing fields, particularly solar shortwave radiation products, are still rare. Estimates based on the same raw data can differ significantly in their annual mean by 40–60 W m^{-2}, due to different methods of data processing (e.g., Chen et al. 1994a). It was decided to use the solar shortwave radiation data from Li (1995), though it shows differences larger than 40 W m^{-2} relative to the Oberhuber climatology (Oberhuber 1988) (cf. Figs. 3a,b). The Li (1995) data covers the years 1985–90, which restricted the model integrations to this period.

Figure 2 shows the annual mean heat flux correction $Q_{correct}$ for the experiments with tidal mixing, taken from year 20 of the spinup. Figure 2 divided by 100 also maps the departure of model SST from the Reynolds annual mean. With this interpretation, one sees that the model SSTs were within 0.5°C of observed values over most of the tropical band (20°N–20°S), but that departures of up to 3°C occur in western boundary currents and the Antarctic Circumpolar Current. These correspond to values of $Q_{correct}$ of well over 50 W m^{-2}, thought to be the maximum error in observed heat flux climatologies. The sum of longwave and sensible heat loss in Eq. (1) is quite accurate in the Tropics, but omits peaks in the Kuroshio and Gulf Stream seen in Oberhuber (1988) and other climatologies. Another possible reason is the inadequate resolution of details of SST in the western boundary currents and the Southern Ocean.

Note that the heat flux correction shows a strong bias toward a heat release through the ocean's surface, that is, compared to the Reynolds SST, the model SST is too high generally. Exceptions are the Gulf Stream, the eastern Pacific, and few patches in the Southern Ocean. The most likely source of this bias is the solar shortwave radiation, which is too strong generally by perhaps 25–50 W m^{-2}. This problem is believed to be due to inadequacies in the radiative models used to infer surface shortwave radiation from satellite reflectance (J. Garrett 1997, personal communication).

In the tropical latitude band between 20°N and 20°S, the flux corrections are of the order 40 W m^{-2}. This is the area where SST anomalies are believed to have the greatest effect on the atmosphere. However, experience shows that interannual anomalies of fluxes are often quite good, even when the long-term means contain large errors (Stockdale et al. 1993).

The seasonal heat flux correction of the Indian Ocean shows little change over the year. Its largest amplitude evolves at the Somali Current region with strongest heat uptake during the Southwest Monsoon and weak heat loss in boreal winter (not shown).

Tests of this heat flux formulation with the tropical IMET time series of heat fluxes (Weller and Anderson 1998) are described in Godfrey and Schiller (1997).

c. Experimental strategy

We have performed two experiments, experiment SF (seasonal forcing with tidal mixing in the Indonesian

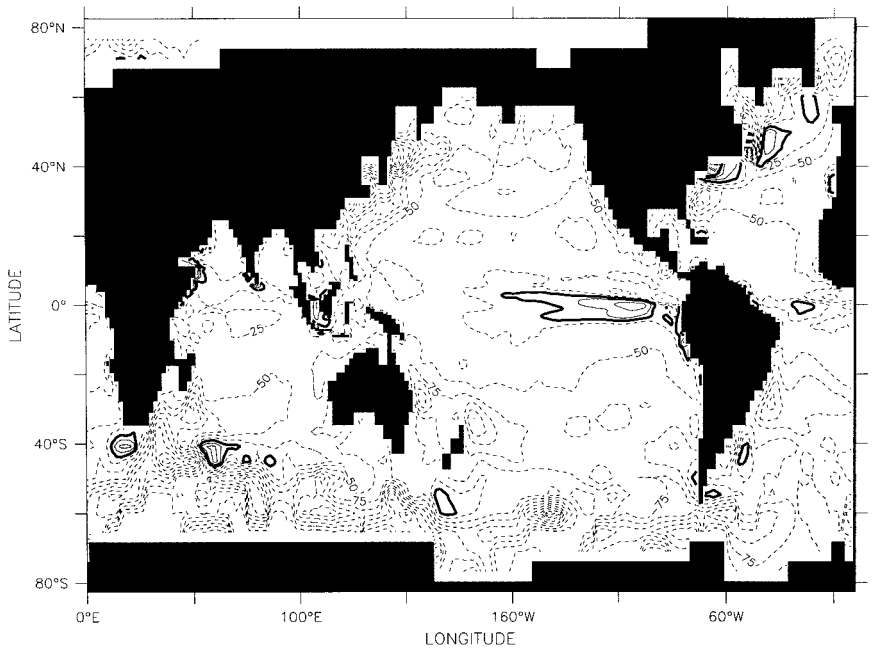

FIG. 2. Annual mean heat flux correction for experiments with tidal mixing (SF), $Q_{correct}$ (W m^{-2}). These numbers, divided by 100, are also the difference between observed and modeled annual mean SST in degrees Celsius.

area) and experiment SFN (seasonal forcing without tidal mixing in the Indonesian area). For the experiments described in this paper, all time-dependent datasets are seasonal climatologies (including surface wind stresses, solar shortwave radiation, heat flux correction, specific humidities, sea surface salinity, and restoring profiles for Red/Mediterranean Sea outflow). The seasonal climatologies for the wind stresses and the solar shortwave radiation were calculated by averaging the respective interannual forcing fields over the period 1985–90. For comparison with interannual forcing experiments, the seasonal experiments were integrated over the same period of 6 years. Although the drift of the model's thermocline in 6 years under seasonal forcing conditions is tiny, we have diagnosed the first 2 years after the spinup (an output of instantaneous fields at the middle of each month was used). To compare forcing fields and observations (which are based on monthly averaged quantities) with instantaneous model fields and based on experience, we assume that the model fields are representative of monthly averages and that it has little variability below the monthly timescale. Annual means have been calculated by averaging 12 instantaneous values.

3. Seasonal climatology of the upper Indian Ocean

The first focus of this paper is on the adequacy of our model physics and flux formulations for reproducing the complex observed monsoonal cycle in the upper Indian Ocean, especially its thermal structure. Since the emphasis of this paper is on the seasonal variability in the Indian Ocean, annual mean fields are only considered when appropriate. A more thorough discussion of annal mean circulation properties of the Indian Ocean can be found in Godfrey et al. (1995). These sections describe the most realistic experiment, SF.

a. Heat flux

While this paper is concerned with modeling seasonal behavior in the Indian Ocean, the longer-term aim of this work is to predict interannual SST anomalies. We therefore need to know the accuracy of the mean seasonal estimates of net heat flux obtained from the first three terms of Eq. (1), compared to available climatologies. This can provide a rough ''quality control'' on the reliability of the interannual variations. We might expect interannual flux anomalies to be about as accurate (in fractional terms) as the mean seasonal fluxes, at least on a component-by-component basis.

Figure 3a shows the annual mean shortwave radiation, according to Oberhuber (1988); Fig. 3b shows the mean shortwave radiation for 1985–90 according to the ISCCP ''bulk'' estimate (Li 1995). As noted earlier, the ISCCP estimate is as much as 40 Wm^{-2} higher. However, in fractional terms the errors in the annual mean (and in the mean seasonal cycle, not shown) are of order 20%, so we might expect similar errors in interannual anomalies of shortwave radiation. Figures 3c and 3d show the annual mean latent heat loss from Oberhuber (1988) and from our model. The good agreement here, and in the mean seasonal equivalents (not shown), is

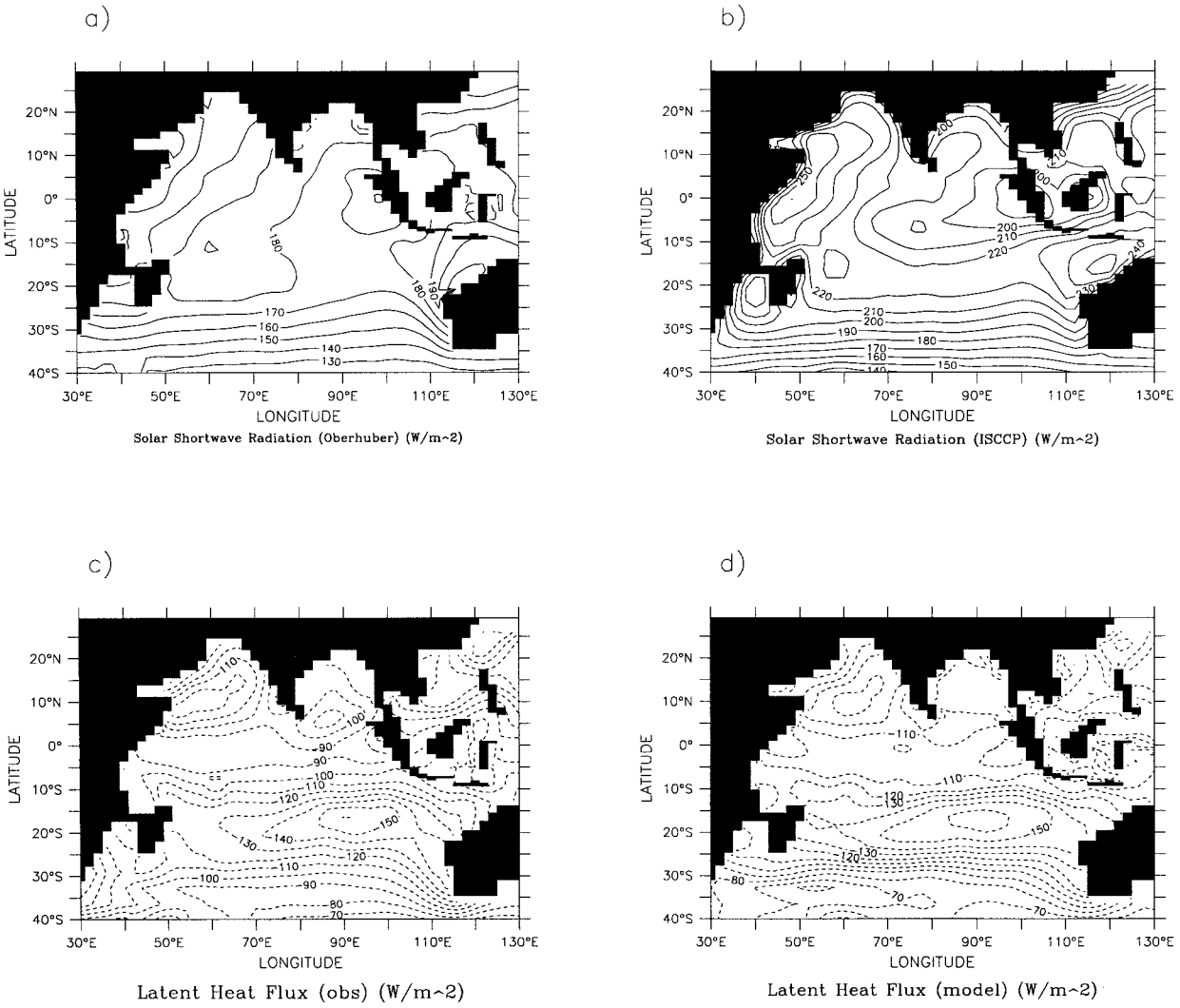

FIG. 3. Annual mean net shortwave radiation from the (a) Oberhuber (1988) climatology and (b) ISCCP dataset. Annual mean latent heat flux from the (c) Oberhuber (1988) climatology and (d) from the model (experiment SF). C.I. = 10 W m^{-2}. Positive heat flux into the ocean.

partly because the humidity ratio δ in Eq. (1) is a function of position and season. The differences mainly reflect those between FSU and COADS wind speeds. Similar plots of the sum of longwave radiation and sensible heat loss (not shown) indicate that they are quite well represented by the model. Thus, the difference (Fig. 4a) between the first three terms of Eq. (1) and the annual mean heat flux due to Oberhuber comes mainly from the shortwave radiation. This appears as high as 20–40 W m^{-2} compared to the Oberhuber estimate, over much of the Indian Ocean.

Figure 4b shows the difference between the annual mean heat flux Q_{tot} and the Oberhuber estimate of annual mean net heat flux. According to Eq. (1), Fig. 4b is also the sum of the flux correction $Q_{correct}$ and the flux difference of Fig. 4a. The flux differences of Fig. 4b are smaller than those of Fig. 4a over much of the ocean; that is, the heat flux correction appears to compensate for the high ISCCP values. However, Fig. 4b shows large values near the Somali, Agulhas, and Leeuwin Currents, presumably due to defects in ocean model physics in these regions. Figure 4c shows the annual mean heat flux into the model. It shows heat uptake north of 10°S and a weak heat loss in the southern Indian Ocean subtropics. Note the heat uptake in the ITF area, which is mainly caused by tidal mixing (see below).

Figures 5 and 6 show the seasonal cycle of net surface heat flux from the model and observations (Oberhuber 1988), respectively. Note that the annual mean in Fig. 4c is small compared to the amplitude of the seasonal heat flux. The difference south of 10°S between Oberhuber's climatology and the model's is dominated in all seasons by a heat flux into the ocean, which is strongest in August.

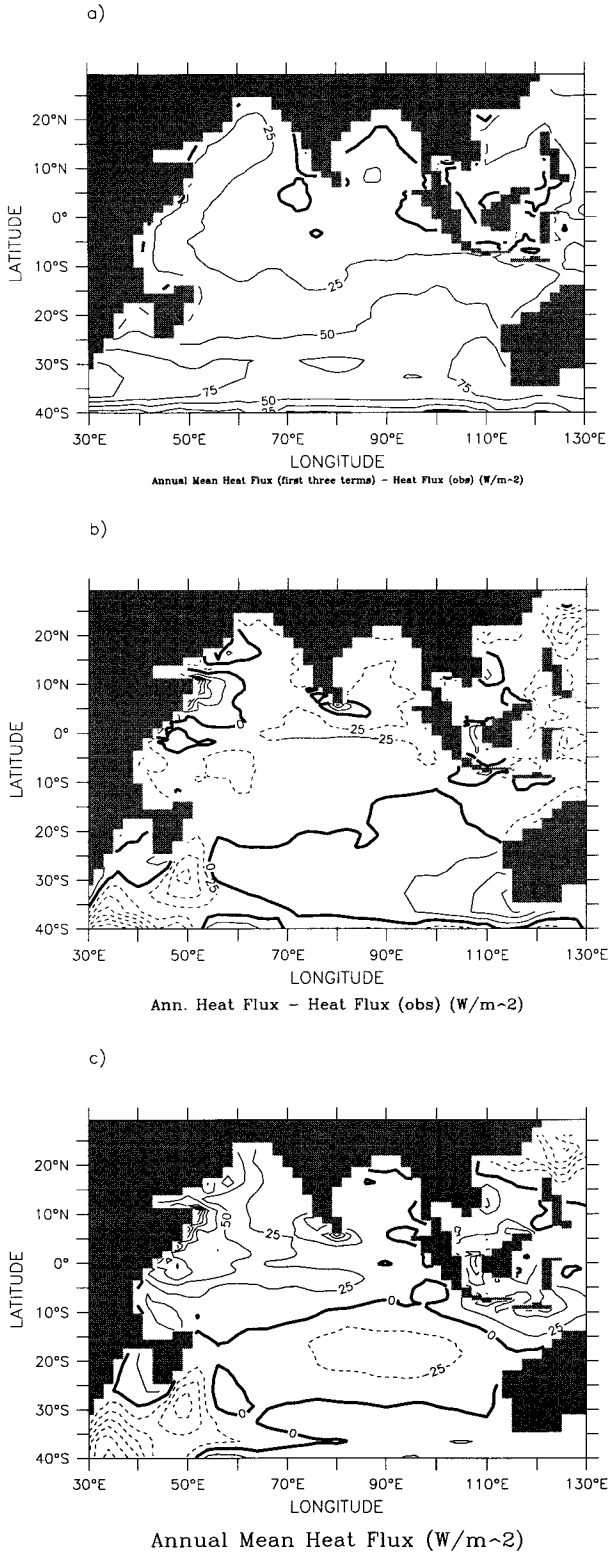

FIG. 4. (a) Annual mean surface heat flux from the first three terms on the right of Eq. (1) of experiment SF minus the Oberhuber (1988) climatology. (b) Annual mean net surface heat flux of experiment SF minus the Oberhuber (1988) climatology. (c) Annual mean net surface heat flux of experiment SF. Positive heat flux into the ocean. C.I. = 25 W m^{-2}.

The net heat fluxes north of 10°S show a more complex (semiannual) signal which is strongly influenced by the monsoons. In February, observed and modeled fluxes are relatively uniform over the region. The observed fluxes [Fig. 6a, and also Chart 72 of Hastenrath and Lamb (1979, hereafter HL)] show a broad maximum extending southwestward from southern India. A similar, though weaker band, is seen in Fig. 5a. The region of high heat flux in Fig. 5a near (3°S, 40°E) is not seen in either climatology.

With the onset of the Southwest monsoon in May (Fig. 5b), cold water is upwelled along the Somalian, Arabian, and Sri Lankan coasts, resulting in strong heat gain. However, over the equatorial northern Indian Ocean, high winds and cloudiness lead to heat loss. A well-defined band of heat gain occurs just south of the equator. These features are just discernible in the Oberhuber climatology (Fig. 6b); they appear much more clearly in HL Chart 75.

In August, in both model and observation, strong oceanic heat gain occurs in the upwelling regions. However, the model heat gain here, and the heat loss in the northeastern Indian Ocean, are exaggerated compared to Fig. 6c and HL Chart 78.

In November, as in February, the pattern of surface heat flux is again relatively uniform. Moderate heat loss occurs in the northern Arabian Sea and the Bay of Bengal, but this is again exaggerated in the model.

In general, the model does a fairly satisfactory job of reproducing the seasonal pattern of net heat flux into the Indian Ocean within the uncertainty of the observations, though the model tends to exaggerate observed maxima and minima.

Wacongne and Pacanowski (1996, hereafter WP) have shown that in their model, the zonally integrated heat transport is dominated by the vertical overturning cell in the northern Indian Ocean. Our streamfunction patterns north of 8°S (the latitude of the Indonesian Throughflow) are qualitatively similar to theirs, in the top 500 m (Fig. 7). Away from the equator, surface Ekman transport is southward in May and August; weakly northward in November and February. A shallow overturning cell is seen across the equator in all months, with surface flows in the opposite direction to the Ekman transport at higher latitudes; as in WP, this cell serves to carry the Ekman flow across the equator, against contrary meridional winds. Note that this cell extends to depth 60 m in May—that is, below the minimum mixed layer depth at that time (Fig. 8b); thus the upwelling arm of this cell should bring cold water into the surface mixed layer. This may be responsible for the patch of heating just south of the equator, in Fig. 5b. By contrast, the similar cell in August (Fig. 7c) is shallower than the minimum mixed layer depth at that time (Fig. 8c), which may explain the absence of a band of heating south of the equator in Fig. 5c.

Inflow is seen below 200 m in May and August, feeding the coastal upwelling at various coastal sites in the

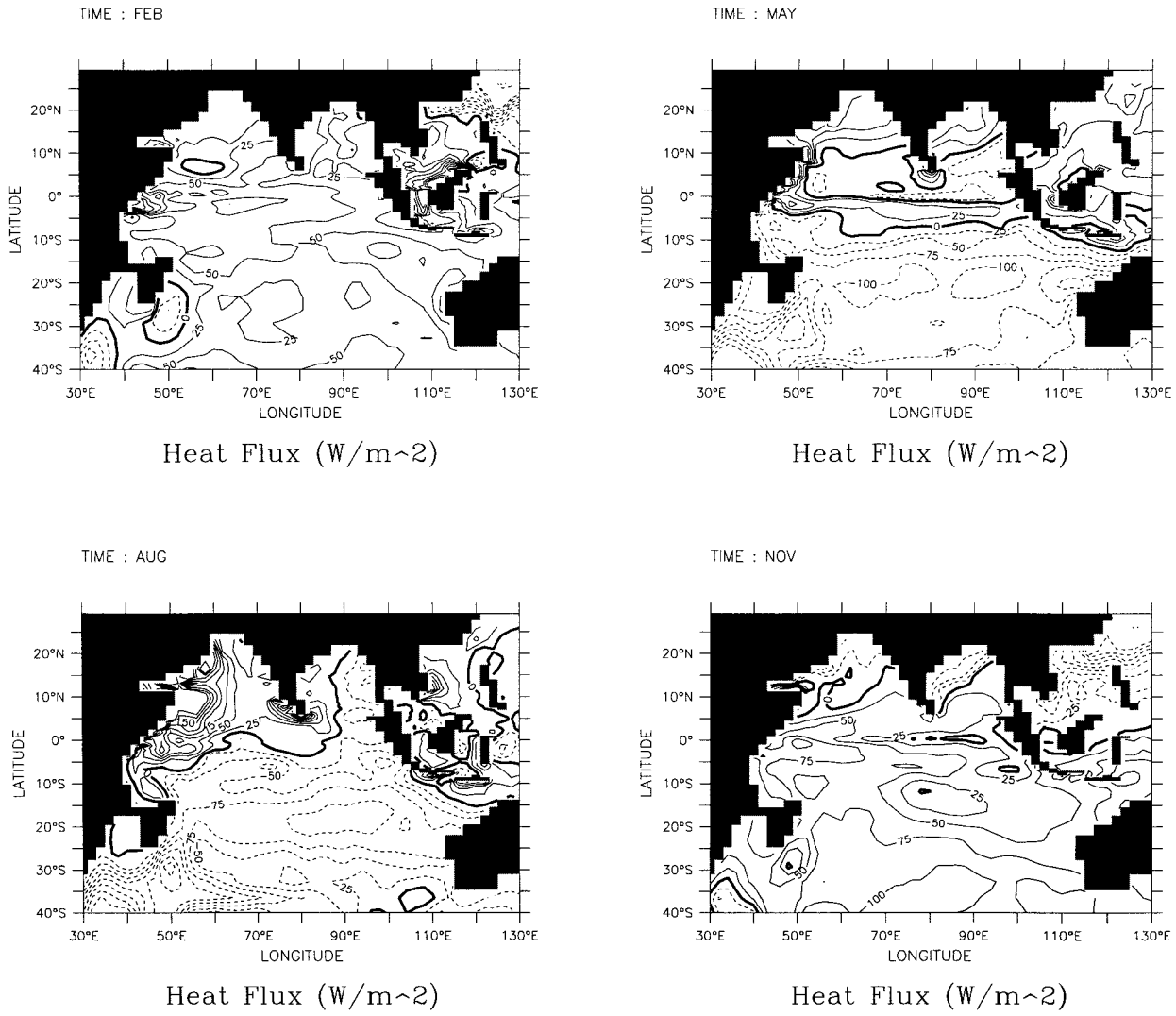

FIG. 5. Net surface heat flux of experiment SF for (a) February, (b) May, (c) August, and (d) November. C.I. = 25 W m^{-2}.

northern Indian Ocean. As in WP, this inflow does not simply reverse in November and January; it downwells to deeper levels, particularly near the equator. In effect, this downwelling along the equator stores incoming thermocline water in the East African Current through the northern winter, to be upwelled off the northern coast of the Indian Ocean the following summer.

Due to the heat flux correction the modeled SST is close to Reynolds and Smith's (1994) SST, with typical differences of less than 0.5°C. Larger differences are found in the areas of the western boundary current (model SSTs too low) and the southern Indian Ocean around 30°S (model SSTs too high; not shown, cf. Fig. 2).

b. Mixed layer depth

Rao et al. (1989) describe the seasonal variations of the mixed layer depth (MLD) in the Indian Ocean. Godfrey et al. (1995) found that the main features of these variations could be qualitatively understood by inspection of the seasonal wind fields, especially Ekman divergence, and surface heat fluxes. Figure 8 shows the model mixed layer depth in February, May, August, and November, while Fig. 9 shows the same maps from Rao et al. (1989). Rao et al. defined the MLD to be the depth at which temperature was 1°C lower than that at 10-m depth. The model MLD of Fig. 8 is defined the same way, except that the temperature of the top level was substituted for the temperature at 10 m. In alternative maps (not shown), model mixed layer depth was defined as the depth at which density was 0.5 higher than in the top level. The resulting MLDs were 10–20 m shallower than those of Fig. 8 in regions of known ''barrier layer'' formation (Sprintall and Tomczak 1992), like the Bay of Bengal, and somewhat deeper in regions of high evaporation like the northern Arabian Sea. However, the patterns were very similar.

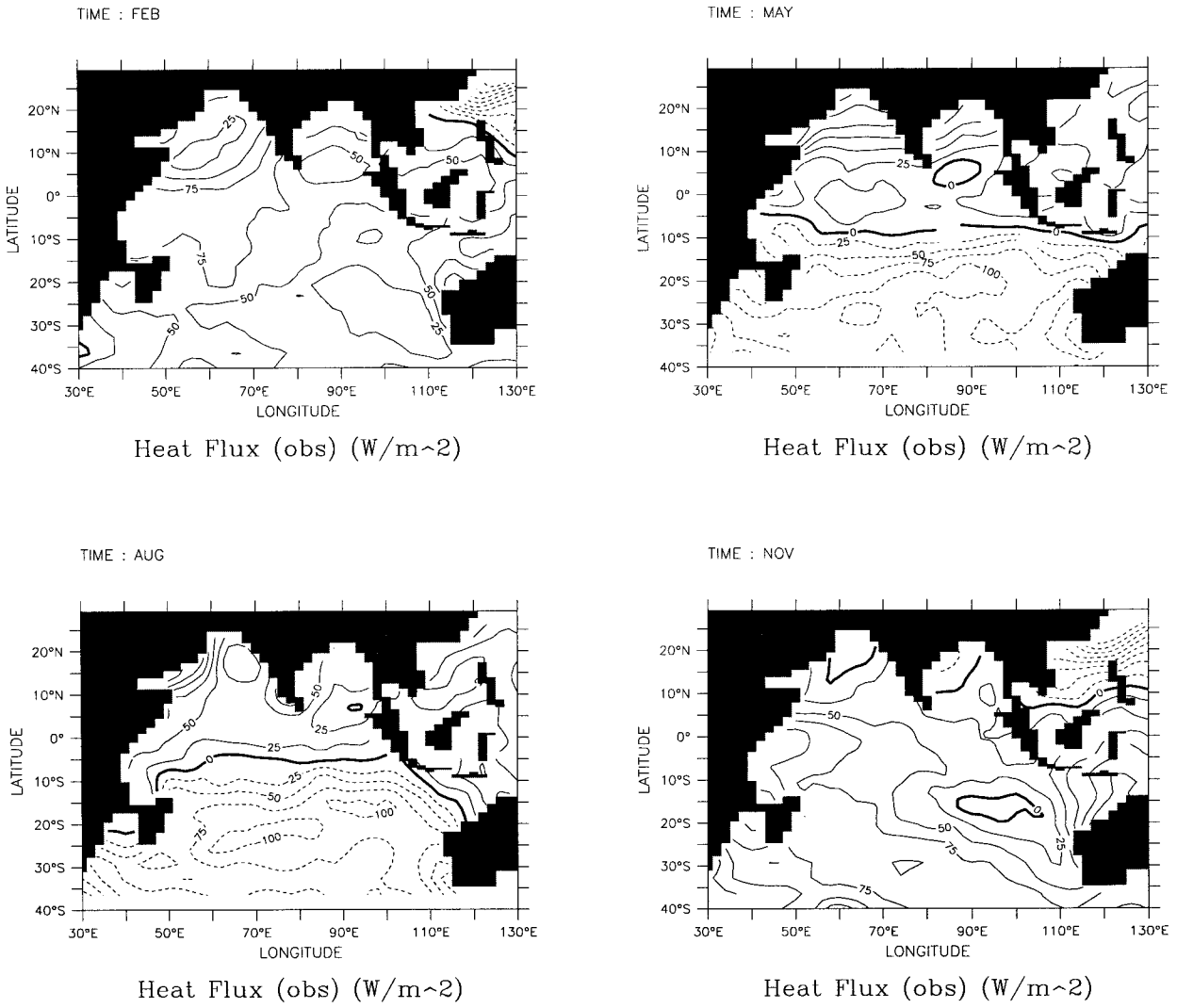

FIG. 6. Observed net surface heat flux from Oberhuber (1988) for (a) February, (b) May, (c) August, and (d) November. C.I. = 25 W m^{-2}.

Comparison of Figs. 8 and 9 suggests that the model is generally quite successful in simulating the observed seasonal patterns of MLD north of 25°S, with maxima and minima of MLD in essentially the correct places in each season; though model MLD is too deep near 20°S at the Australian coast in November.

A short run of the model was performed with the factor of 0.4 in Eq. (3) replaced by 1.0, resulting in a 2.5-fold increase in the magnitude of shortwave radiation through any given level. This caused mixed layers to deepen unrealistically by about 20 m. Similar sensitivity of mixed layer depth to transparency change is reported by Latif et al. (1994).

c. Surface steric height

Geostrophic currents can affect SSTs by causing horizontal advection, so we need to test the realism of the model's seasonally varying patterns of surface geostrophic flow. Here we define steric height as dynamic height divided by the acceleration due to gravity *g* (e.g., Tomczak and Godfrey 1994). This definition makes steric height have dimensions of height. We have prepared maps of the model's surface steric height relative to 513 m at three-monthly intervals and also similar maps based on Levitus and Boyer (1994) data relative to 500 m. We do not show these because the seasonal variations are only strong in the Northern Hemisphere, and here these seasonal maps are similar in pattern to the MLD maps of Fig. 8; and also to the maps of upper layer depth (h1) in McCreary et al. (1993, hereafter MKM). All three can be used qualitatively to indicate the direction and relative strength of near-surface geostrophic flow. The only notable differences between our steric height patterns and MKM's h1 in the Northern Hemisphere are (i) the lack of a southeastward flow along the west coast of India in February in our model, probably due to our relatively coarse (2°) zonal resolution;

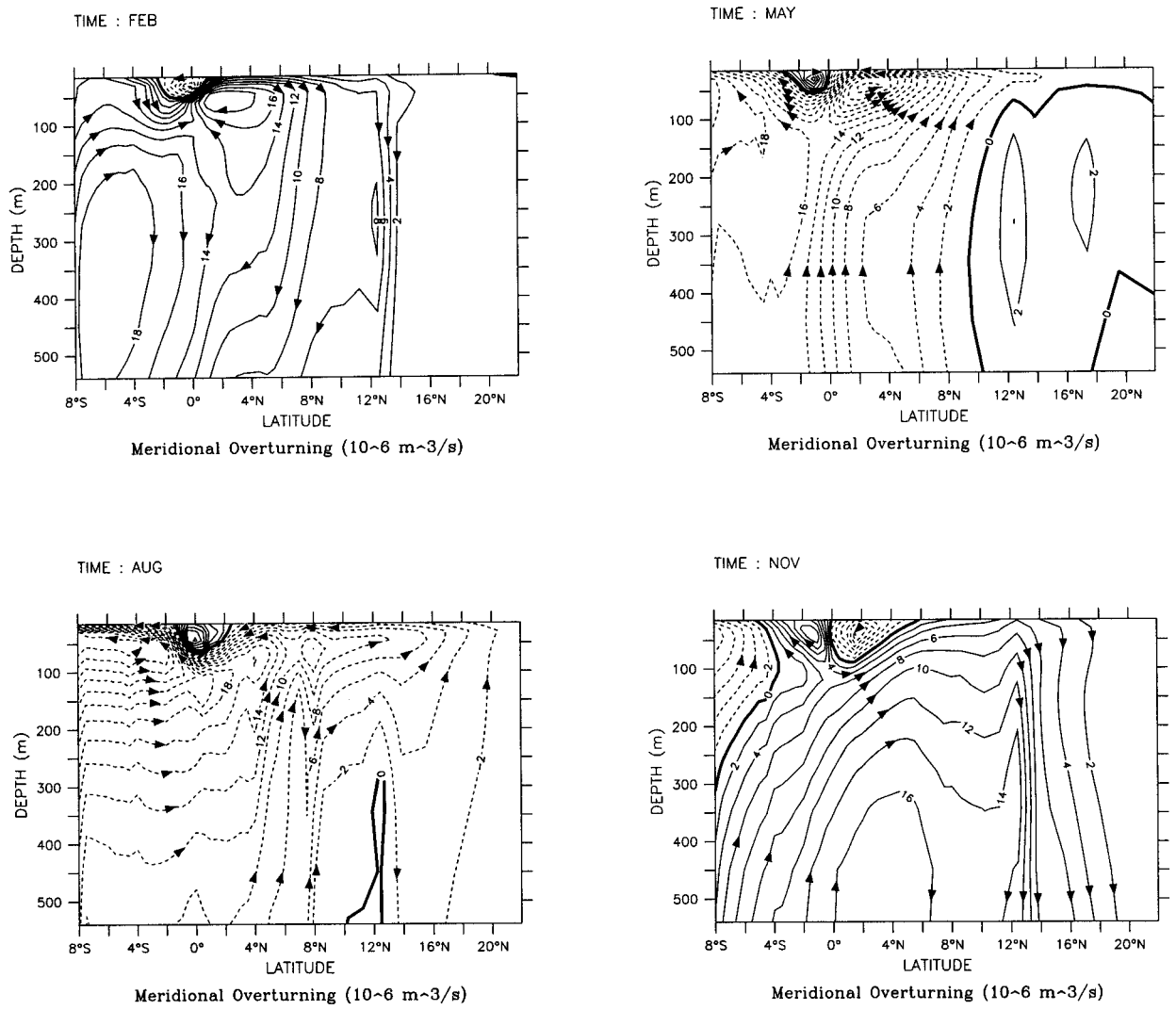

FIG. 7. Seasonal cycle of near surface meridional streamfunction in the Indian Ocean north of 8°S (the latitude of the Indonesian Throughflow) for experiment SF. (a) February, (b) May, (c) August, and (d) November. Positive (negative) values indicate clockwise (counterclockwise) transports. C.I. = 2.0 Sv. Arrows indicate direction of circulation.

(ii) in the Bay of Bengal our model shows northwestward flow in August, while the observations show northeastward flow [see McCreary et al. (1996) for a discussion of four mechanisms that may cause flows in this region]; and (iii) the absence of a throughflow in MKM. We refer readers to MKM and McCreary et al. (1996) for a discussion of the seasonal dynamics of flow in the northern Indian Ocean, merely noting that our results are broadly consistent with theirs.

Throughout the year, Fig. 10 shows an offset of about 10 cm because the model's thermocline is too thick, but agreement of slopes is generally quite good. The main discrepancy occurs in August along 90°E; inspection of the seasonal maps show that this discrepancy is a quite local effect compared to neighboring longitudes. Such differences may as well be due to paucity of data as to model inadequacies. Another seasonal effect of interest is the strong annual Rossby wave, driven near 15°S by the seasonally varying curl between the steady trades to the south and the monsoon winds to the north. These waves cannot be seen in Fig. 10, but our model results are consistent with observations (Masumoto and Meyers 1998) and with earlier model studies (Perigaud and Delecluse 1993). At the western boundary, the model East African Coastal Current is strongest in August and weakest in February, but is present all year, in accord with observations (Schott et al. 1990).

In the southern subtropics, seasonal variations of steric height are relatively small, so Fig. 11 (which shows observed and modeled annual mean steric heights, relative to 500 and 513 m, respectively) serves well to illustrate them throughout the year. MKM's patterns of h1 (and of surface velocity) do not show the eastward surface flow that feeds the Leeuwin Current, probably

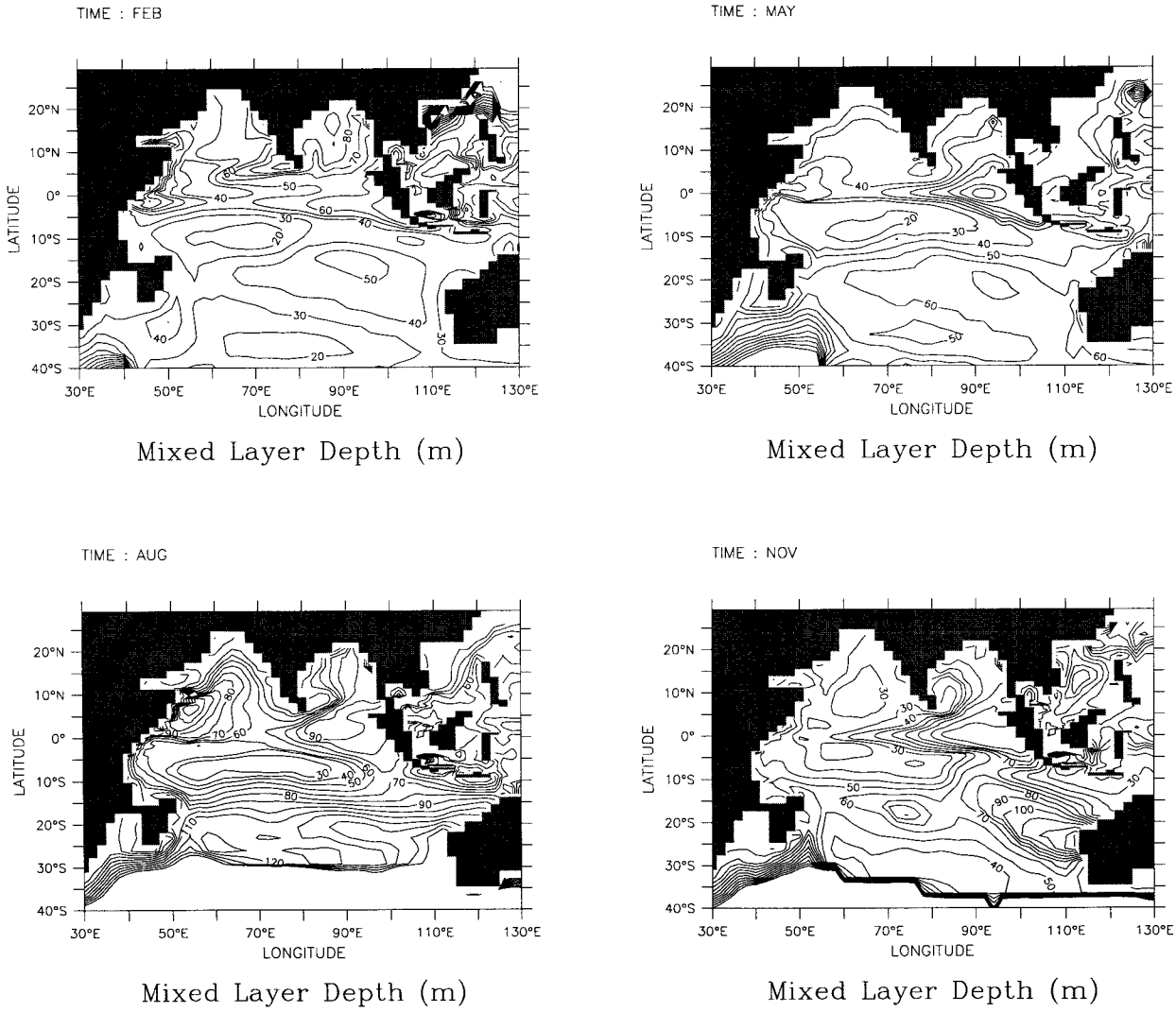

FIG. 8. Mixed layer depths of experiment SF for (a) February, (b) May, (c) August, and (d) November. The MLD was defined by the depth at which temperature is 1°C less than that of the top level (7.5 m). C.I. = 10 m.

mainly because they have no Indonesian Throughflow to maintain high steric heights off northwestern Australia (e.g., Godfrey and Weaver 1991). The model captures the strong eastward geostrophic flow quite well. However, the model also shows unrealistically low steric heights west of Madagascar, resulting in a southward flow from Madagascar, which is much too strong compared to observations. We believe this is primarily due to the fact that the Mozambique Channel is blocked in our model. Another possible explanation might be that, in blending FSU winds north of 30°S with Hellerman and Rosenstein winds south of 30°S, we could have introduced spurious wind stress curls. However, we tested this explicitly before running the model, and (to our surprise) found no wind stress curls at this latitude that looked unrealistic, either seasonally or on annual mean.

4. Indonesian Throughflow: Mass and heat transports

a. Annual mean throughflow

The model was compared to the geostrophic throughflow as estimated by expendable bathythermograph (XBT) measurements (Meyers et al. 1995) along a section from Australia (Shark Bay) to Java (Sunda Strait). The model's annual mean geostrophic flow distribution relative to 700 m (Fig. 12) qualitatively has all the features of the observations shown in Fig. 13 except for the 1-Sv Leeuwin Current. This may be because the model resolution at the southern end of the section is too coarse to resolve this boundary current. The model has, however, a weak southward geostrophic flow down to 100 m, which is more than offset by a strong north-

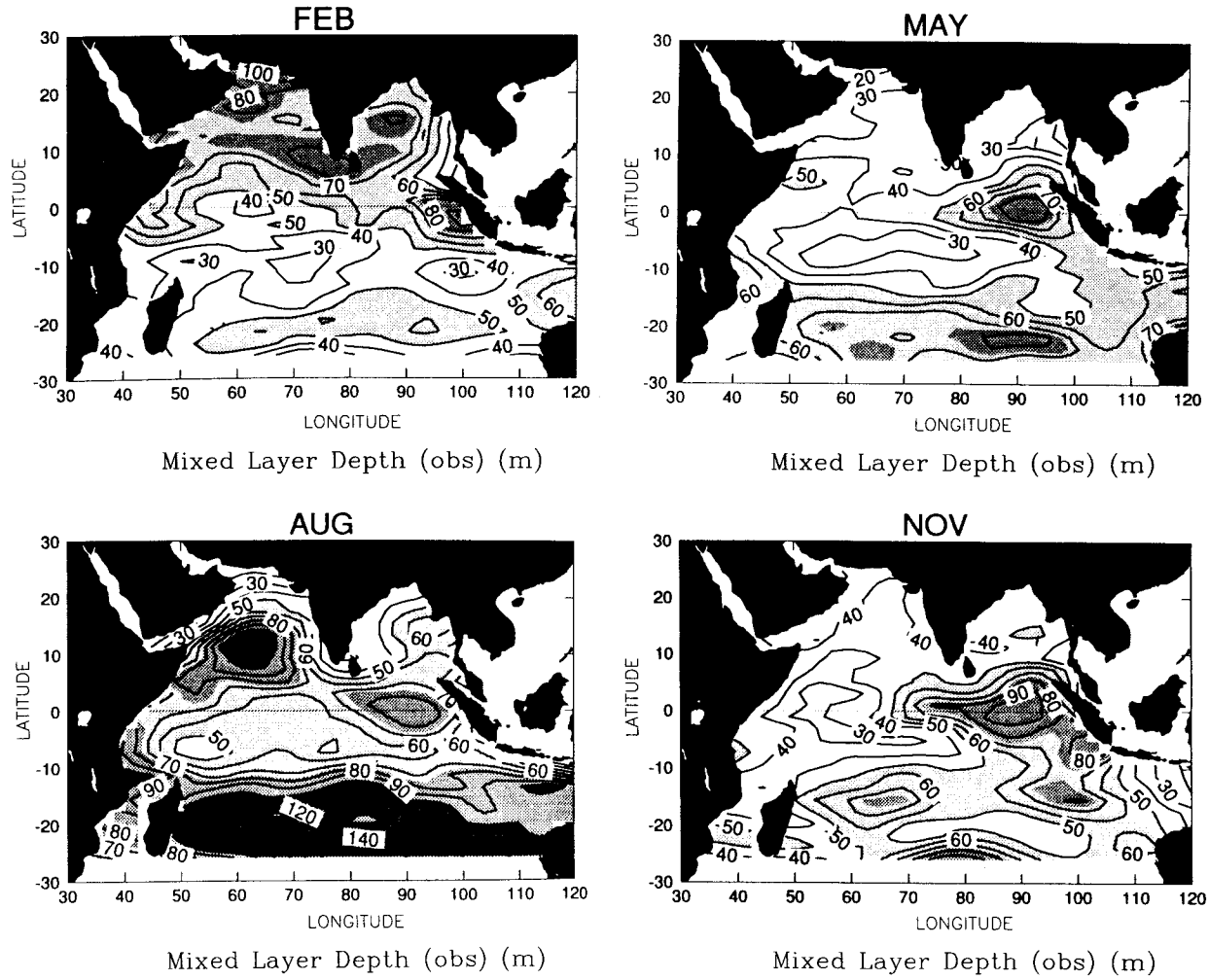

FIG. 9. Mixed layer depths from Rao et al. (1989) for (a) February, (b) May, (c) August, and (d) November. The MLD was defined by the depth at which temperature is 1°C less than at 10 m. C.I. = 10 m.

ward undercurrent. Figure 12 shows two South Java Currents, split vertically into two cells like the observations, and a weak westward undercurrent beneath the surface's northeastward flow, south of the main throughflow. The model has less northeastward flow south of the main throughflow (1.5 Sv for the observations, less than 1 Sv for the model). In the model, the main throughflow extends between 200 and 1000 km offshore from Java and is 11 Sv; in the observations it extends only from 300 to 800 km offshore and is 8 Sv. The model has a South Java Current of 0.7 Sv, compared to the present estimate of 2 Sv from observations. The observed South Java Current may decrease when one uses local observations of salinity, rather than the coarse-grid averages used in obtaining Fig. 13. Taking the numbers as they are, the observed mean geostrophic transport relative to 700 m is 4 Sv, while the model gives 9.7 Sv. In the model, the velocity at depth H (700 m or the bottom), and its area integral, only yield a notable contribution between 100 and 1000 km away from the coast of Java (i.e., just below the core of the throughflow) of 1.7 Sv. The annual mean velocity pattern below 700 m (Fig. 14) extends down to 2200 m and can be traced up to 1200 km away from the South Java coast. Below the throughflow is a weaker undercurrent: its core is located on the continental shelf of Java. Along the Australian North West Shelf, weak currents flow southward. The deep flow from the Indian Ocean toward the Timor Sea is a regional feature: there is only a weak annual mean flow (<1 Sv) eastward around the southeastern tip of Timor. The total transport below 700 m in the model equals 1.4 Sv westward. The Ekman contribution is 3.5 Sv, which gives a total model throughflow transport of 16.3 Sv.

From Australia to within 500 km of Java, geostrophic flow relative to 750 db from Levitus and Boyer (1994) data (not shown) is qualitatively like the model and XBT results. However, the Levitus and Boyer (1994) data show a strong westward jet near Java. This results in a net transport of 14 Sv relative to 750 db. We speculate

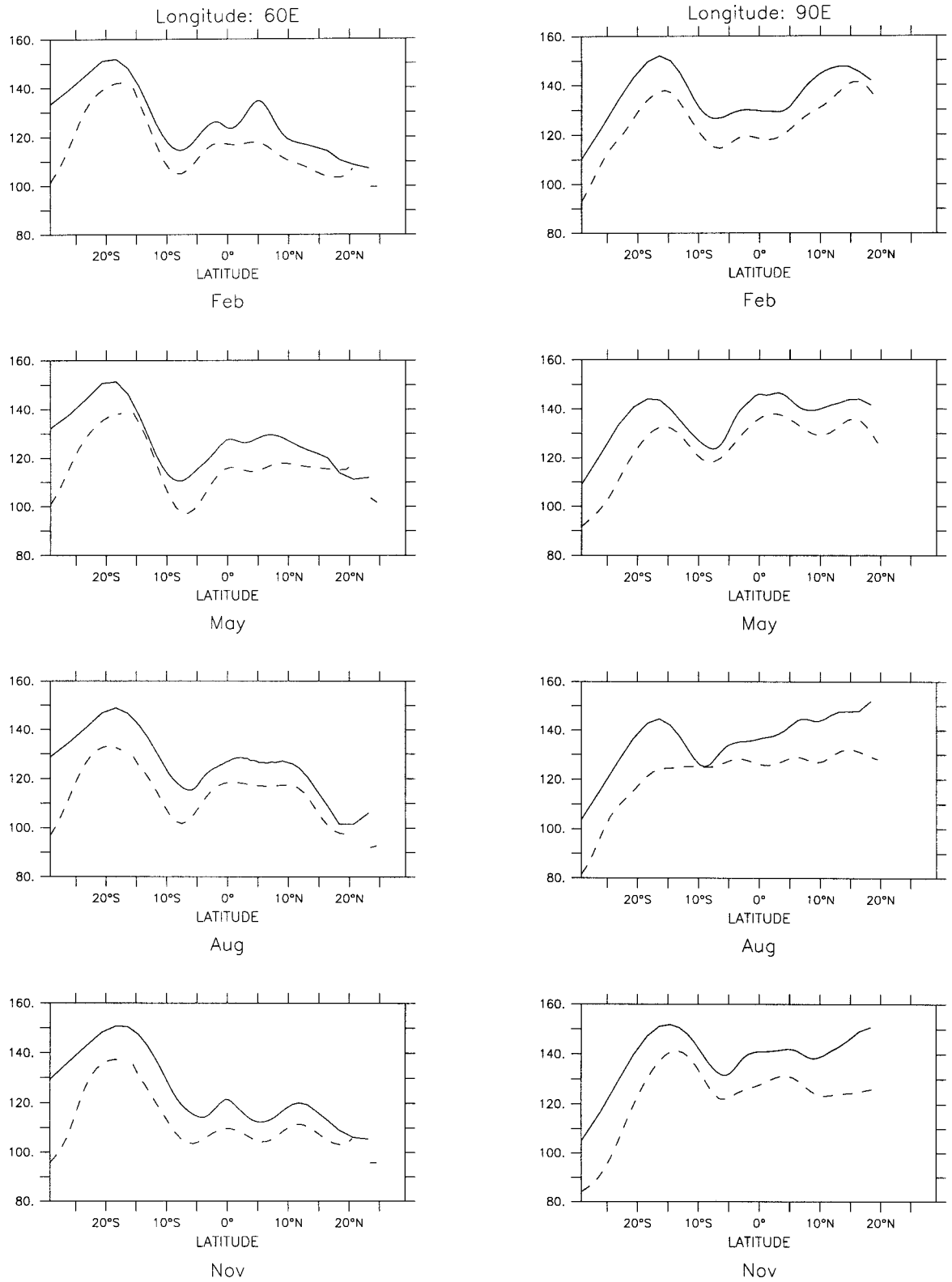

FIG. 10. Modeled (solid line) and observed (dashed line) surface steric height relative to 513 and 500 m, respectively. Observations are from Levitus and Boyer (1994). Left column: section along 60°E, right column: section along 90°E. (a), (e) February, (b), (f) May, (c), (g) August, and (d), (h) November.

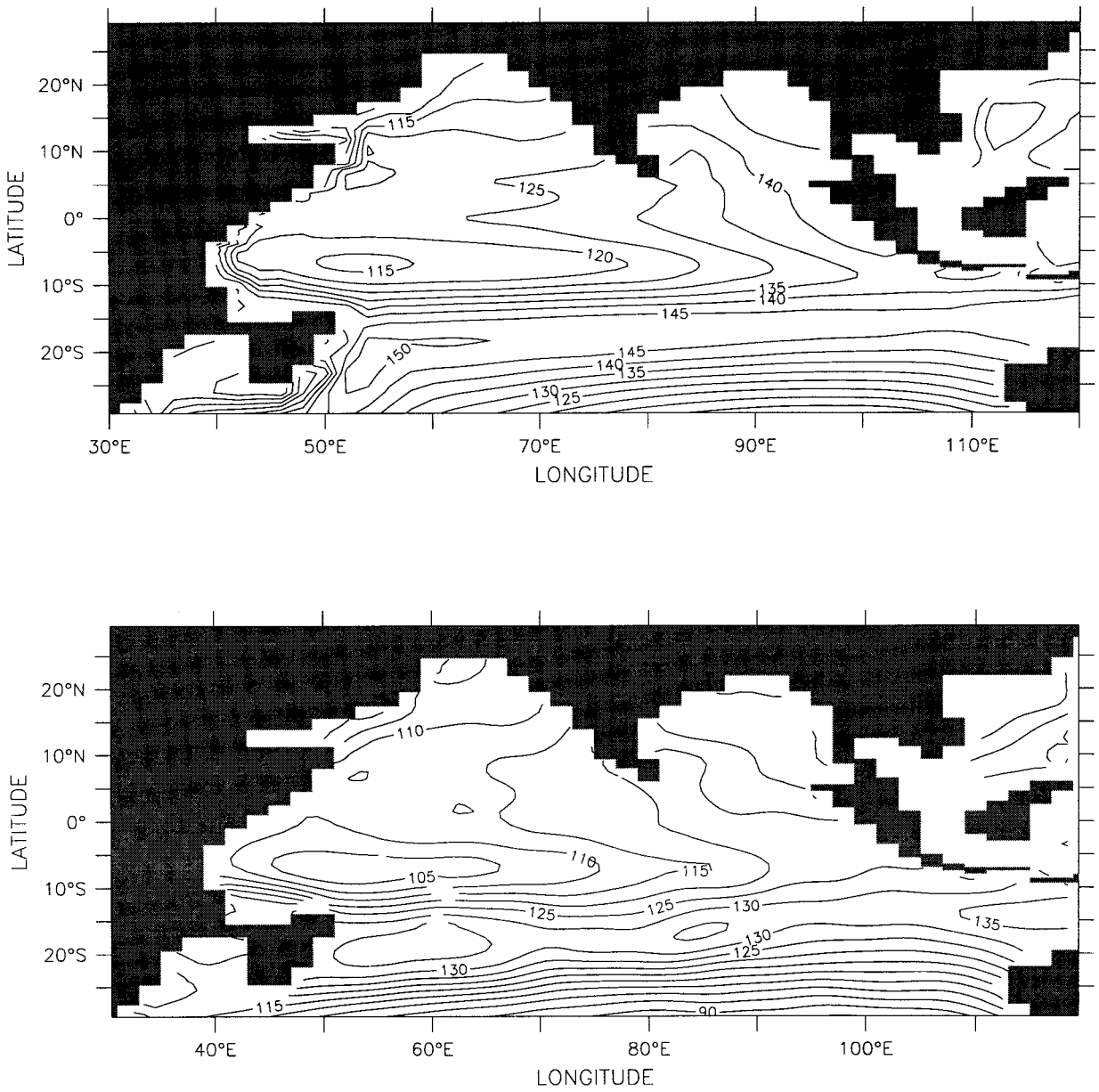

FIG. 11. Annual mean surface steric height (a) from the model (experiment SF), relative to 513 m; (b) from Levitus and Boyer (1994) relative to 500 m. C.I. = 5 dyn cm.

that Levitus may have averaged data from north of Java, trying to get values close to Java, but that would reduce the ITF magnitude rather than increase it!

Maps of depth-integrated steric height (DISH) relative to 1000 m (not shown) show flat regions west of Sumatra and west of Australia. This implies a geostrophic throughflow of $(g\Delta\text{DISH})/f(12°\text{S}) = 10 \pm 1$ Sv, in close agreement with the model value relative to 700 m. It is worth noting that both in the XBT observations and the model, the South Java Current is strongest nearly 200 km from the coast. This suggests that the South Java Current may already be a zonal jet, rather than a coast-hugging current, at the northern end of the IX1 section.

The annual mean net transport of the model through the Indonesian archipelago includes the contributions from Lombok Strait and the Timor Sea as defined above. However, the mean transport in the model is 16.3 ± 2.0 Sv. This is high relative to the observations summarized by Wijffels et al. (1996), but is close to the ''Island Rule'' value, as often found in numerical models (e.g., Godfrey 1996; Schneider and Barnett 1997).

b. Mean seasonal cycle of throughflow

The seasonal cycle of total transport in the model (full line, Fig. 15) has a maximum in September (18.4

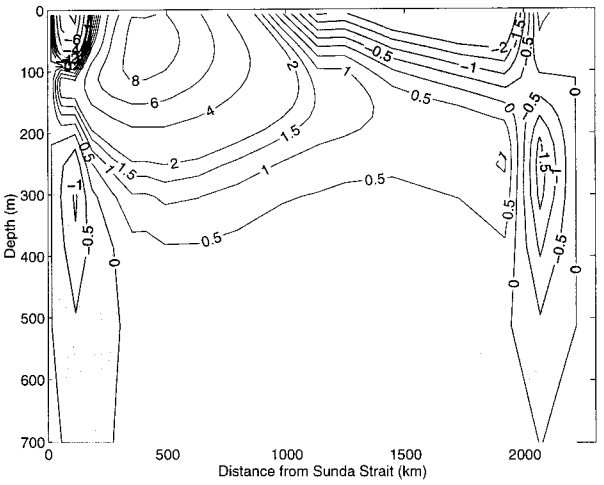

FIG. 12. Annual mean geostrophic velocity (0/700 m) across IX1 section from the model. Shaded areas denote flow from the Indian to Pacific Oceans. Units are cm s^{-1}.

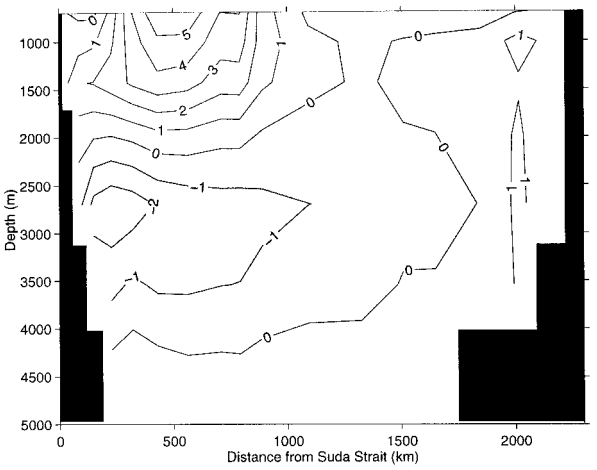

FIG. 14. Annual mean total velocity below 700 m across IX1 section from the model. Shaded areas denote flow from the Indian to Pacific Oceans. C.I. = 1 mm s^{-1}.

Sv), a secondary maximum in March/April (18.1 Sv), a minimum in February (12.9 Sv), and a range of about 5 Sv. The pecked line shows the result of applying the island rule (Godfrey 1989), $T_I = \oint \tau^{(l)} dl(f_N - f_S)$, using instantaneous seasonal winds. As in Masumoto and Yamagata (1996), the island rule has some skill at seasonal timescales. Curiously, the full model throughflow appears to lead the instant island rule estimate. The same feature can be seen in Schneider and Barnett (1997, their Fig. 17); in their model they show that the throughflow magnitude is primarily due to the difference between a term due to the integral of the wind stress around the island rule path and a term from bottom pressure torque integrated over the interior of the island rule path. The latter lags the former, so when its contribution is removed, the resulting throughflow leads the wind integral.

The phases of the geostrophic transport relative to a depth of 700 m match those of the observations (Meyers et al. 1995) shown in Fig. 15 surprisingly well. The maximum in geostrophic transport in August and the minima in May and November occur in both model and observations. The secondary maximum in the model in January is one month earlier than the observed maximum. Although modeled and observed phases are almost identical, their magnitudes are not. As noted earlier, the annual mean geostrophic transport in the model is more than twice the observed value. Figure 15 reveals that this relative difference exists throughout the year, with smallest and largest differences in November (<1 Sv) and August (>9 Sv), respectively. Another notable

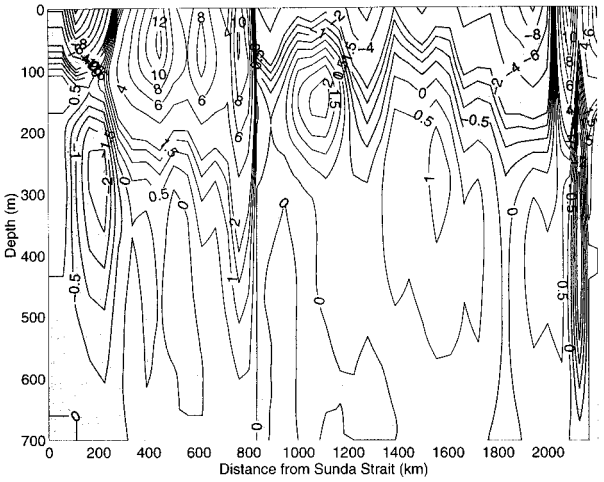

FIG. 13. Annual mean geostrophic velocity (0/700 m) across IX1 section from XBT data using *T–S* relation from Levitus and Boyer (1994) projected onto XBT line. Shaded areas denote flow from the Indian to Pacific Oceans. Units are cm s^{-1}.

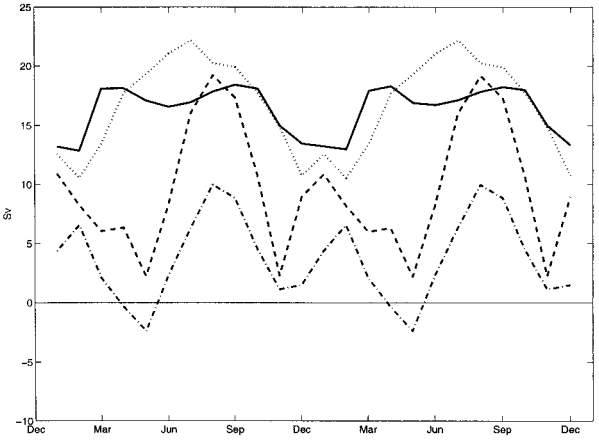

FIG. 15. Seasonal cycle of ITF transport across IX1 section from the model. Solid: net throughflow from the model; dotted: net throughflow calculated with island rule (Godfrey 1989); dashed: geostrophic transport (0/700 m) from the model; dash–dotted: geostrophic transport (0/700 m) from observations (Meyers et al. 1995).

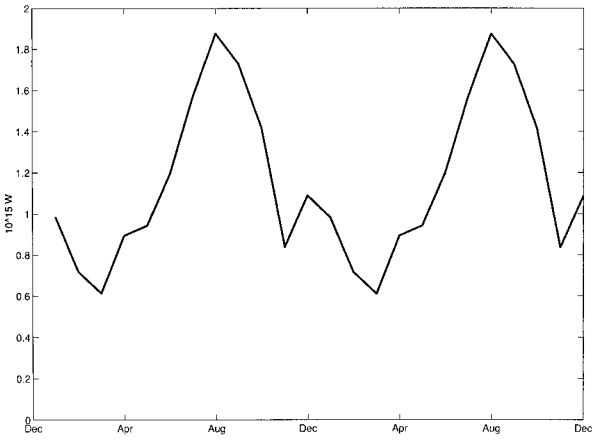

FIG. 16. Seasonal cycle of net heat transport across IX1 section from the model. Units are in PW ($=10^{15}$ W). Positive values denote transport from the Pacific to Indian Oceans.

feature are the large semiannual variations in both the modeled and observed geostrophic transports, which are much larger than in the total transport. This indicates that the geostrophic transport relative to 700 m does not represent a reasonable estimate for the net throughflow, since it does not account for the important contributions from the reference level, the deep transport below 700 m, and the Ekman transport. Note, that the increased tidal mixing slightly decreased the net throughflow by about 0.3 Sv; that is, it changed the barotropic (and baroclinic) structure of the ITF transport.

c. Heat transport

Figure 16 shows an estimate of the net heat transport across the IX1 section from the model, based on the assumption that the return flow south of Tasmania has the model's depth-averaged temperature of water between southern Tasmania and 50°S, whose average value was 3.72°C. It should be noted that this choice is arbitrary; there is no well-defined way to separate returning Indonesian Throughflow waters from those of the Antarctic Circumpolar Current. Another choice [such as Schneider and Barnett (1997) choice of 3.4°C] would add a multiple of the barotropic mass transport of Fig. 15 to the heat transport curve of Fig. 16; but for physically reasonable values of the return flow temperature (an upper limit is the transport-weighted temperature from Tasmania to 50°S of 8.56°C, and a lower limit is 0°C), the qualitative features of Fig. 16 are unchanged.

With our choice of return flow temperature, the annual mean heat transport from the Pacific to the Indian Ocean is 1.15 PW (1 PW = 10^{15} W). The seasonal heat transport has a similar phase to the baroclinic volume transport above 700 m (dashed line, Fig. 15): it does not resemble the variations of the barotropic transport (full line, Fig. 15). This reflects the fact that in our model [as found by Schneider and Barnett (1997)] the ''baroclinic'' component of the heat transport (in the sense of Hall and Bryden 1982) is comparable to or larger than the ''barotropic'' component, and the former has a much stronger seasonal cycle. The heat transport of Fig. 16 is smallest in March (0.58 PW) and largest in August (1.86 PW). Compared to the model's annual mean southward heat transport across 7.75°S (this latitude encompasses a closed basin with mass conservation) of 0.45 PW, the ITF transport of 1.15 PW toward the southern Indian Ocean is significantly larger than the contribution from the northern and tropical Indian Ocean. Furthermore, the heat transport from the Pacific to the Indian Ocean represents a strong sink of heat for the Pacific warm pool region (Hirst and Godfrey 1993).

5. Impact of tidal mixing

The Indonesian archipelago with its irregular topography, numerous sills, extensive shelves, and large tidal currents is suitable for large dissipation of tidal energy. Using a simple advection–diffusion model, as well as hydrographic and satellite data, Ffield and Gordon (1992, 1996) demonstrated the strong impact of tidal mixing in the Indonesian area on water mass properties over the whole water column. Figure 17 shows five annual mean potential temperature–salinity curves along the main path of the ITF (the seasonal variations are relatively weak and therefore not discussed here). The cumulative effect of tidal mixing is clearly visible as one follows the path of the water masses from the Makassar Strait (Fig. 17a, ''●'') via the bifurcation point of the throughflow (Fig. 17b, ''○'') to the center of tidal mixing in the Banda Sea (Fig. 17c, ''*''). Note also the very weak vertical salinity gradient in the Timor Sea (Fig. 17d, ''+'') in comparison to the strong gradient in the Makassar Strait. The slight increase in salinity, which is particularly visible in the Lombok Strait profile (Fig. 17e, ''×''), is due to deep undercurrents toward the coast with low salinity that augment their salinity by tidal mixing. The modulation of water masses in the ITF by tidal mixing is at least in qualitative agreement with the *T*–*S* diagrams of Ffield and Gordon (1992, their Fig. 3).

Figure 17 also reveals a decrease in SST due to tidal mixing of up to 0.5°C in the Timor Passage, which reduces the difference between modeled and observed SST (Reynolds and Smith 1994) to less than 0.3°C in that area (not shown). The flux correction Q_{correct} was calculated separately for experiments SF and SFN (seasonal forcing with and without tidal mixing, respectively), by relaxation to Reynolds SST with a 100 W m^{-2} relaxation constant, so this small SST difference implies a large difference in surface heat flux. Figure 18 clearly shows this signal: without tidal mixing there is only a weak heat gain in the Banda Sea and Timor Passage (Fig. 18a), but with tidal mixing (Fig. 18b) the area shows a strong increase in ocean heat uptake (Fig.

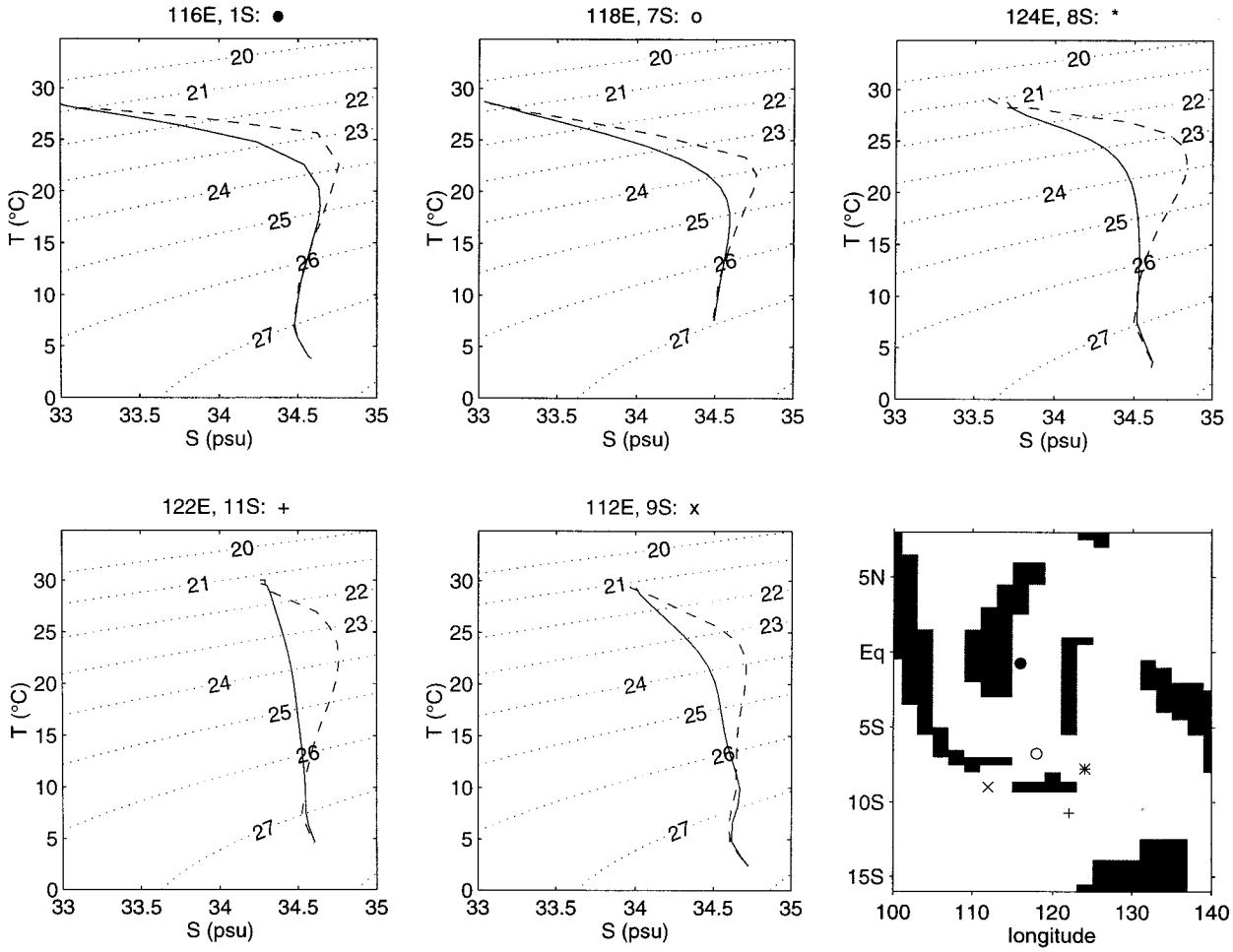

FIG. 17. Annual mean potential temperature–salinity curves in the Indonesian Throughflow area. Solid lines: experiment SF; dashed lines: experiment SFN. A label (●, ○, *, +, ×) shown above each panel indicates the five profiles in Fig. 19f.

18c), which exceeds 60 W m^{-2} south of Timor, leading to an annual average heat flux of over 80 W m^{-2}. Heat flux climatologies (e.g., Oberhuber 1988) support this model result.

Both Figs. 18a and 18b show a large heat flux correction west of Kalimantan, which cancels out in the difference (Fig. 18c). This feature is almost entirely due to a large flux correction in February. At this time strong northeasterlies blow along the Kalimantan coast, generating vigorous upwelling (in the model), with cold upwelled water transported into the shallow Java Sea. This oceanic process appears exaggerated compared to reality. Curiously, a similar situation of large offshore Ekman transports occurs off the south coast of Irian Jaya in August, yet large flux corrections—indicative of problems with model physics—do not develop in this case. Evidently, important aspects of model physics depend on quite subtle details of local topography. Such results serve as a reminder that the heat budget of the topographically complex Indonesian region needs to be handled carefully, and our results will need confirmation from models that treat tidal mixing in a physically more rigorous way than has been possible for us.

Given the changes in surface heat flux, a modification to the depth of the ocean's mixed layer can also be expected. Using a criterion based on vertical density differences, the cooling of the near-surface water masses becomes apparent in the reduction of the mixed layer depth. Figure 19 shows the annual mean difference between experiments SF and SFN. Although changes in mixed layer depth are only of the order of 10 m, these numbers represent about 20% to 30% of the seasonal mixed layer depth. Thus, tidal mixing contributes to a closer agreement of modeled and observed mixed layer depths in the ITF area (Figs. 8 and 9).

We have examined maps of heat flux and mixed layer depths for the entire Indian Ocean and there is no significant change outside the region of the maps shown. To summarize, enhanced vertical mixing in the Indonesian Throughflow has two important regional consequences: First, it mixes warm and fresh surface waters with the underlying cooler and saltier water masses, and

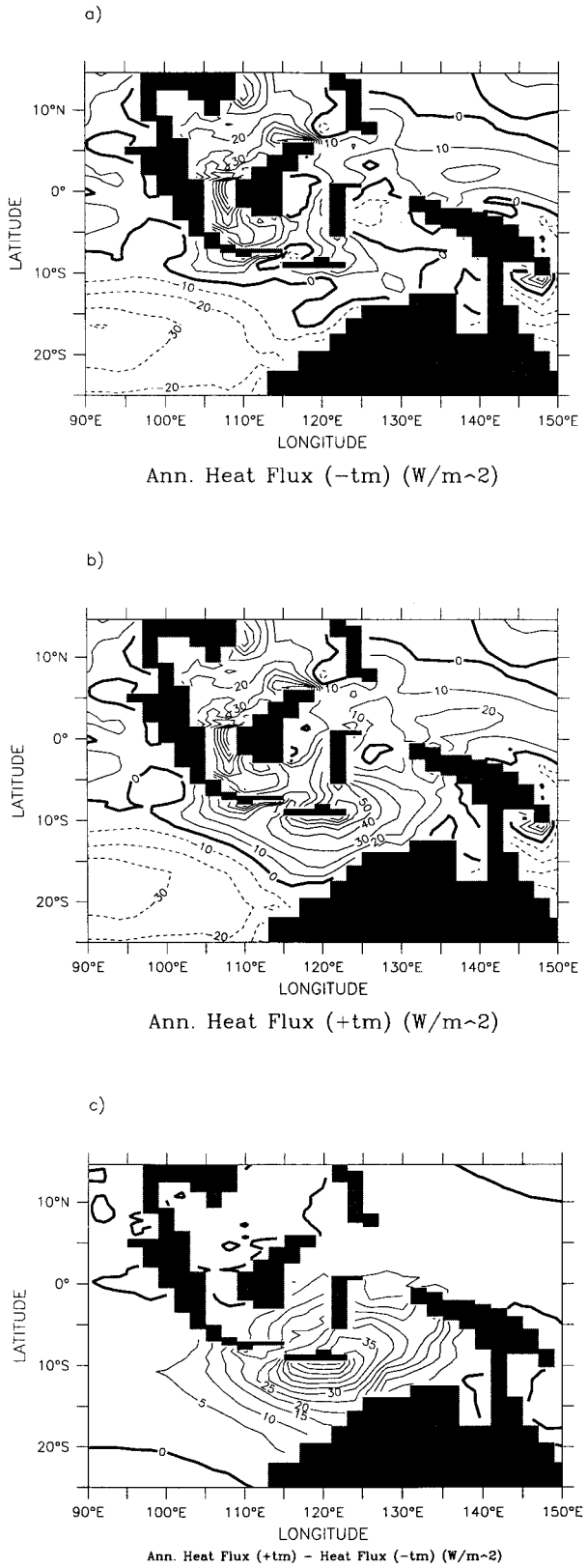

FIG. 18. Annual mean net surface heat flux of (a) experiment SFN, (b) experiment SF (C.I. = 10 W m^{-2}). (c) The difference of (b) minus (a) (C.I. = 5 W m^{-2}).

therefore affects the buoyancy budget of the ITF water before it is exported to the Indian Ocean. Second, the reduction of SST caused by strong vertical mixing affects the ocean–atmosphere heat fluxes that are needed to bring the model's SST close to the observed values. In a coupled ocean–atmosphere model without artificial strong restoration toward observed SST, we anticipate that the neglect of tidal mixing will result in SSTs that may be more than 2°C too high in the Indonesian region, thereby changing the topography of the 28°C isotherm in the warm pool. This could significantly change the coupled model's performance.

How does the simulated tidal mixing affect the Indian Ocean? The *T*–*S* profiles (Fig. 17) suggest that effects of tidal mixing are advected along the throughflow into the Indian Ocean. Figure 20 shows a section along the central latitude of the throughflow (10.7°S) of the difference in potential temperature across the Indian Ocean in the upper 1000 m, between experiment SF and SFN, from East Africa to the Timor Passage. The whole basin is affected by tidal mixing, with the strongest signal in the Timor Passage and on the Australian shelf, where potential temperature differences exceed 1.5°C just below the mixed layer and velocity increases by about 2 cm s^{-1} [total velocities are O(10 cm s^{-1})]. The temperature and velocity differences gradually decrease toward the western Indian Ocean, but the tongue of lower temperatures still exceeds 0.1°C off the African coast. This cooling of the near-surface water masses brings the model's thermocline closer to observations and thus reduces the heat flux correction by about 50 W m^{-2} in the Indonesian area, in agreement with our flux correction [Eq. (4)]. Below 190 m, the downward mixing of warm surface waters causes an increase in thermocline temperature. Again, the strongest signal is found off the Australian shelf where potential temperatures increase by more than 0.5°C at depth 350 m. To further illustrate the impact of tidal mixing on the Indian Ocean, Fig. 21 shows the change in salinity at depth 142 m (in the model, this depth coincides with the depth of the 20°C isotherm in the eastern Indian Ocean). The downstream effect of tidal mixing is determined by the mean advection. At the center of tidal mixing salinity differences exceed 0.3. Following the path of the throughflow, the water masses join the westward South Equatorial Current, the differences decreasing as the distance from the Banda Sea increases, and are finally ''reflected'' eastward through the South Equatorial Countercurrent and the Indian Monsoon Current (this also holds for the seasonal differences, although they are modified by the monsoonal circulation system). Note that the East Madagascar Current advects the tidal mixing signal into the South Atlantic and Southern Ocean. Similar spreading of the signal into the Indian Ocean is found at deeper levels with the maximum amplitude shifted toward 20°S in the Leeuwin Current region (not shown). Although the model results are in fair agreement with observations, the simplified parameterization of tidal mixing is

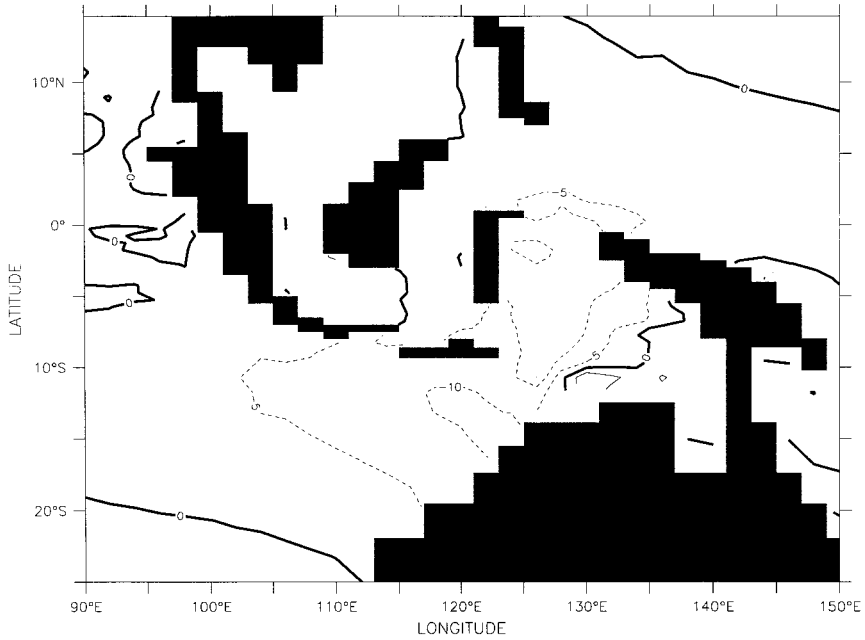

FIG. 19. Annual mean difference of mixed layer depths of experiment SF minus experiment SFN. The MLD was defined by the depth at which potential density σ_Θ is 0.5 kg m^{-3} less than that of the top model level. C.I. = 5 m.

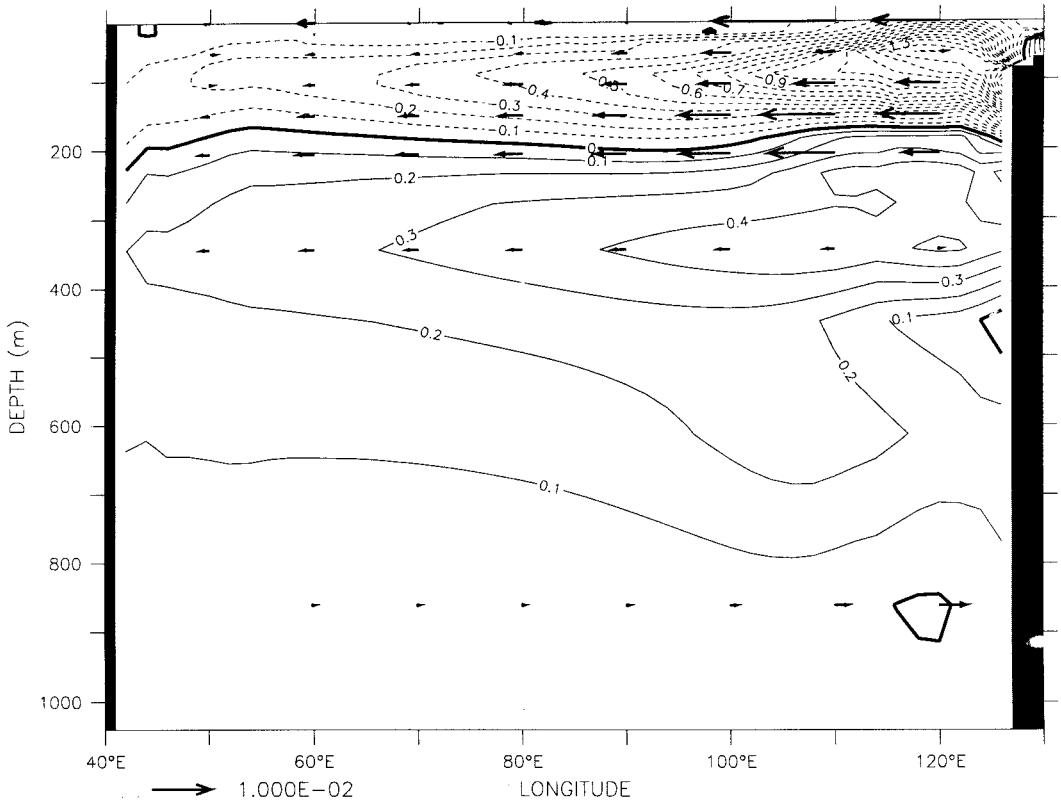

FIG. 20. Annual mean difference of potential temperature of experiment SF minus experiment SFN along 10.7°S. C.I. = 0.1°C. Superimposed are the differences of some velocity vectors in the zonal/vertical plane between experiment SF and experiment SFN. The reference arrow (in m s^{-1}) is shown at the lower left edge of the plot.

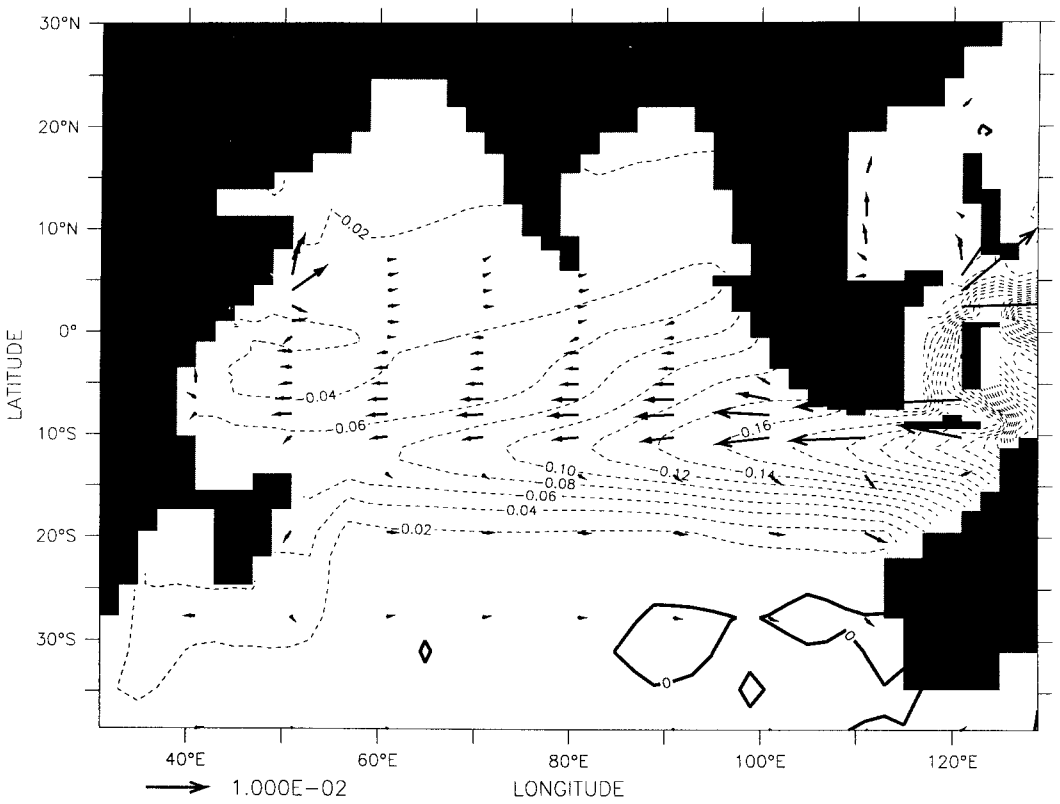

FIG. 21. Annual mean difference of salinity of experiment SF minus experiment SFN at 142-m depth. C.I. = 0.02. Superimposed are the differences of some horizontal velocity vectors between experiment SF and experiment SFN. The reference arrow (in m s^{-1}) is shown at the lower left edge of the plot.

model dependent and requires further improvements in the future.

6. Summary and discussion

A global ocean circulation model with enhanced tropical resolution has been used to study the impact of the Indonesian Throughflow on the Indian Ocean. Particular care has been employed in choosing a surface heat-flux boundary condition so that in interannual runs of the model we can hope to obtain physically reasonable SST anomalies and to analyze their physical mechanisms. We therefore discuss the accuracy of the model's seasonal cycle of surface heat fluxes and of its seasonally varying mixed layer depths. The model's spatial pattern of the Indonesian Throughflow and the seasonal variations of its total mass transport were both compared with observations, and the seasonal variations of the heat transport into the Indian Ocean were calculated.

We find that our model does a reasonable job of simulating the seasonally varying currents and mixed layer depth of the Indian Ocean. However, flux corrections in upwelling regions were too large, presumably because the upwelled water was too cold. This was notable in the Somali Current (Figs. 5a,c), the upwelling branch of the cross-equatorial cell in May (Fig. 5b), and west of Kalimantan. This behavior is puzzling, given that the mixed layer depths are well-simulated: it may be a function of the coarse horizontal spacing of the model.

Nevertheless, the results suggest that the model should adequately simulate interannual SST anomalies. The errors in model physics are likely to be no worse than the known uncertainties in interannual estimates of heat fluxes and wind stresses.

A reasonable simulation of ocean dynamics in the Indian Ocean and the Indonesian Throughflow requires a reliable simulation of the seasonal cycle of surface fluxes. We applied a heat flux parameterization to the model that depicts with reasonable accuracy the surface heat flux in tropical areas away from western boundary currents. Typical errors (i.e., heat flux corrections) of the annual mean within the 20° latitude belt are less than 50 W m^{-2} (equivalent to a SST error of less than 0.5°C). Despite using state-of-the-art parameterizations and forcing fields, errors introduced by the combination of datasets from different sources inevitably led to inconsistencies in the seasonally forced experiments. We could identify two major sources of error in the external forcing fields. First, the solar shortwave radiation is likely the cause of the large heat flux correction in subtropical areas. Second, there are two problems related to the solar shortwave penetration: the temporal reso-

lution of the data and the vertical resolution of the model. We believe that the use of annual mean solar penetration coefficients prevents a more realistic simulation of the upper 100 m of the ocean. Using a coupled ocean–atmosphere model, Cohen-Solal and Le Treut (1996) recently demonstrated the importance of solar irradiance within the ocean. They showed that the evolution of the mixed layer and SST are strongly influenced by seasonal solar penetration, with a strong sensitivity of SST particularly in the subtropics and midlatitudes of the summer hemisphere. Experiments with annual mean and seasonally variable solar penetration depth produced differences in SST of 2°C in the midlatitudes and of 0.5°C in the equatorial areas. This problem of temporal resolution might be overcome once improved satellite-based bio-optical properties of the oceans become available on a seasonal or even monthly basis (e.g., NASA's SeaWiFS project). The moderate vertical resolution of our model grid is another factor that might contribute to an increased amount of heat storage in the uppermost model layer and thus to a negative heat flux correction.

It was shown that a parameterization of tidal mixing in the ITF region reduced the SST and enhanced the net surface heat flux into the ocean northwest of Australia. This agreed with observations (e.g., Ffield and Gordon 1996) and significantly reduced the model error. It should be noted, however, that this empirical parameterization of tidal mixing is very crude and model dependent.

The simulated tidal mixing complements results from Hirst and Godfrey (1993, 1994) who investigated the global response to an opened and closed ITF. Paths of the perturbed water masses due to tidal mixing are similar to results from Hirst and Godfrey (1994). Although in this paper we do not consider the initial adjustment processes related to tidal mixing, the surprising similarity between these two studies suggests similar adjustment dynamics. The tidal mixing involves the propagation of a coastal Kelvin wave counterclockwise around Australia and its subsequent westward radiation as a Rossby wave into the Indian Ocean. The similarity between the experiments of Hirst and Godfrey (1994) and those described in this paper become even more evident when one looks at the Pacific Ocean. The proximity of simulated tidal mixing to the Pacific in Fig. 1 suggests a modulation of vertical mixing in the Pacific Ocean. This hypothesis is confirmed by the shape of the spreading tidal mixing perturbation signal (not shown); it is very similar to the temperature difference plots due to an opened/closed ITF in the upper thermocline (Hirst and Godfrey 1994; their Figs. 5b and 12). The Pacific signal involves a Kelvin signal along the equatorial waveguide, subsequent poleward propagation along the American coast, and finally, westward propagation as a Rossby wave signal.

Although tidal mixing has a predominantly regional impact, the global penetration of the perturbation signal causes changes in subsurface temperatures and salinities worldwide and therefore has an impact on global-scale ocean dynamics. An example of the remote influence of tidal mixing is the heat flux correction in the eastern Pacific Ocean upwelling region. Cold water from intermediate depths is advected vertically to the surface. The resulting surface water is too cold in the model simulation, and therefore the heat flux correction produces an additional heat input into the ocean (Fig. 2). This heat input is reduced by about 10 W m^{-2} in experiment SF compared to experiment SFN, because the upwelled water is slightly warmer (about 0.1°C). Tidal mixing may also have some impact on global climate change scenarios, where it may influence deep-water formation at high latitudes, but an investigation of this feature is beyond the scope of this paper.

Based on a reduced gravity, primitive equation model on sigma coordinates, a recent study by Murtugudde et al. (1998, submitted to *J. Geophys. Res.*) investigates the seasonal-to-interannual effects of the ITF on the tropical Indo–Pacific basin. They mimic tidal mixing by either increasing the horizontal mixing, using a Shapiro filter in the Indonesian region, or by using the increased horizontal mixing plus increased vertical mixing by applying additional modified convective adjustment every 15 days. Murtugudde et al. mostly study the former case. There are fundamental differences in the behavior of their model with tidal mixing compared to ours. Enhanced horizontal mixing affects the Makassar and Lombok Strait transports while simultaneously reducing the recirculation in the Molucca/Seram/Banda Seas. The net effect is a slight increase (0.5 Sv) in the overall transport into the Indian Ocean. In our model tidal mixing has an opposite effect and slightly decreases the net throughflow (0.3 Sv). However, the most important difference between both models and their tidal mixing parameterization is the lack of any noticable cooling of SST in the Indonesian seas in Murtugudde et al.'s model. This result is in contrast to surface observations (e.g., Gordon 1986; Ffield and Gordon 1996) and observations of deep mixing (Hautala et al. 1996).

The model's barotropic transport has an annual mean of 16.3 Sv and a relatively small, mainly semiannual variation (Fig. 15). The Sverdrup version of the island rule (Godfrey 1996) has moderate skill for simulating these seasonal variations (Masumoto and Yamagata 1996); the departures may be due to bottom pressure torques in the Pacific, as suggested by Schneider and Barnett (1997). However, these barotropic transports differ by 3.1 Sv from the throughflow estimate obtained by assuming a ''depth of no motion'' at 700 m and adding the Ekman transport; this is unfortunate, because the latter can be compared directly with observations. The model and observed estimates based on 700 db have similar seasonal cycles, though they have annual means of 13.2 and 7.5 Sv respectively.

The large 3.1 Sv annual mean difference between the model estimate relative to 700 m and the model's true barotropic flow is due to the fact that the model through-

flow through the IX1 section extends well below the sill depth. Figure 14 shows that there are substantial net inflows (or outflows) at most depths below 700 m, right to the bottom (Fig. 14). In the enclosed region east of IX1 such flows imply annual mean vertical flows of up to 1 Sv at some levels—upward near 2000 m, downward near 4000 m—which in turn imply substantial water mass conversion within the enclosed region. We have not explored this surprising result, beyond checking that essentially the same results are obtained in the SF and SFN run; that is, this result does not reflect the effect of tidal mixing. If it is a real effect, it suggests that the choice of a depth of no motion for estimating the throughflow, along lines such as IX1, may not be a simple exercise.

Observational estimates of the heat transport through the ITF are not available. Previous model estimates range from 0.63 PW from the Pacific to the Indian Ocean in the model of Hirst and Godfrey (1993), who used constant mean winds, to 1.08 PW estimated by McCann et al. (1994), who used a 1/2° model with monthly mean climatological wind stresses. Recent analyses of model output from the 1/4° Semtner–Chervin model by Garternicht and Schott (1998, submitted to *J. Geophys. Res.*) and from a coupled ocean–atmosphere model (Schneider and Barnett 1997) both produce a heat flux of 0.9 PW from the Pacific to the Indian Ocean, which is somewhat less than our estimate of 1.15 PW. However, all heat transports depend on the choice of a reference temperature and are therefore arbitrary. Furthermore, the (well defined) southward heat transport across 7.75°S is 0.45 PW, which is close to the value of 0.43 PW in Garternicht and Schott [but both are at the low end of observed values (e.g., Hastenrath and Greischar 1993; Hsiung 1985)]. Those values highlight the importance of the ITF for the heat export toward the southern Indian Ocean.

Acknowledgments. The authors would like to thank R. C. Pacanowski from the Geophysical Fluid Dynamics Laboratory for making the MOM2 code available to us. R. Fiedler's enthusiastic help has been invaluable. During the development of this model we had many stimulating discussions with colleagues at the CSIRO Division of Atmospheric Research and the Bureau of Meteorology Research Centre, Melbourne. In particular, we appreciated the comments of S. Wilson, S. Power, R. Kleeman, T. Hirst, N. Smith, and L. Waterman. We also thank M. Bessell for preparation of some figures. Most of the figures were prepared with the FERRET software package from PMEL.

This project was partly supported by funding from the Department of Industry, Sciences and Technology (CSIRO Climate Variability and Impacts Program) and by a grant from the Land and Water Resources Research and Development Corporation, Australia.

We used the Australian Community Ocean Model (ACOM), which is a synthesis of Australian enhancements and additions to the GFDL Modular Ocean Model [MOM2; (Pacanowski 1995)]. It is a collabrative project between interested ocean researchers in Australia from many organizations. The model code is freely available to any ocean modeler via our Internet address http://www.dmr.csiro.au/acom.

REFERENCES

Blanke, B., J. Neelin, and D. Gutzler, 1997: Estimating the effect of stochastic wind stress forcing on ENSO irregularity. *J. Climate,* **10,** 1473–1486.

Chen, D., A. J. Busalacchi, and L. M. Rothstein, 1994a: The roles of vertical mixing, solar radiation, and wind stress in a model simulation of the sea surface temperature seasonal cycle in the tropical Pacific Ocean. *J. Geophys. Res.,* **99,** 20 345–20 359.

——, L. M. Rothstein, and A. J. Busalacchi, 1994b: A hybrid vertical mixing scheme and its application to tropical ocean models. *J. Phys. Oceanogr.,* **24,** 2156–2179.

Cohen-Solal, E., and H. Le Treut, 1996: Impact of ocean optical properties on seasonal SST: Results with a surface model coupled to the LMD AGCM. *Climate Dyn.,* **12,** 417–433.

Cresswell, G., A. Frische, J. Peterson, and D. Quadfasel, 1993: Circulation in the Timor Sea. *J. Geophys. Res.,* **98,** 14 379–14 389.

da Silva, A. M., C. C. Young, and S. Levitus, 1994: *NOAA Atlas NESDIS 6. Atlas of Surface Marine Data 1994.* Vol. 1: *Algorithms and procedures,* U.S. Department of Commerce. National Oceanic and Atmospheric Administration, 83 pp.

Drosdowsky, W., 1993: Potential predictability of winter rainfall over southern and eastern Australia using Indian Ocean sea-surface temperature anomalies. *Aust. Meteor. Mag.,* **42,** 1–6.

Ffield, A., and A. L. Gordon, 1992: Vertical mixing in the Indonesian thermocline. *J. Phys. Oceanogr.,* **22,** 184–195.

——, and ——, 1996: Tidal mixing signatures in the Indonesian Seas. *J. Phys. Oceanogr.,* **26,** 1924–1937.

Garternicht, U., and F. Schott, 1998: Heat fluxes of the Indian Ocean from a global eddy-resolving model. *J. Geophys. Res.,* in press.

Gates, W. L., and A. B. Nelson, 1975: A new (revised) tabulation of the Scripps topography on a 1° global grid. Part I. Terrain heights, Tech. Rep. R-1276-1-ARPA, The RAND Corporation.

Godfrey, J. S., 1989: A Sverdrup model of the depth-integrated flow for the world ocean allowing for island circulations. *Geophys. Astrophys. Fluid Dyn.* **45,** 89–112.

——, 1996: The effect of the Indonesian Throughflow on ocean circulation and heat exchange with the atmosphere: A review. *J. Geophys. Res.,* **101,** 12 217–12 237.

——, and A. J. Weaver, 1991: Is the Leeuwin current driven by Pacific heating and winds? *Progress in Oceanography,* Vol. 27, Pergamon, 225–272.

——, and A. Schiller, 1997: Tests of mixed layer schemes and surface boundary conditions in an ocean general circulation model, using an equatorial data set, CSIRO Rep. No. 231, CSIRO Division of Marine Research, Hobart, Australia, 60 pp.

——, A. Alexiou, A. G. Ilahude, D. M. Legler, M. E. Luther, J. P. McCreary Jr., G. A. Meyers, K. Mizumo, R. R. Rao, S. R. Shetye, J. H. Toole, and S. Wacogne, 1995: The role of the Indian Ocean in the global climate system: Recommendations regarding the Global Ocean Observing System, OOSDP Background Rep. Number 6, Texas A&M University, College Station, TX, 89 pp.

Gordon, A., 1986: Interocean exchange of thermohaline water. *J. Geophys. Res.,* **91,** 5037–5046.

Hall, M. M., and H. L. Bryden, 1982: Direct estimates and mechanisms of ocean heat transport. *Deep-Sea Res.,* **26,** 339–359.

Hastenrath, S., and P. J. Lamb, 1979: *Climatic Atlas of the Indian Ocean. Part 2. The Oceanic Heat Budget.* University of Wisconsin Press.

——, and L. Greischar, 1993: The monsoonal heat budget of the

hydrosphere–atmosphere system in the Indian Ocean sector. *J. Geophys. Res.,* **98,** 6869–6881.
Hatayama, T., T. Awaji, and K. Akitomo, 1996: Tidal currents in the Indonesian Seas and their effect on transport and mixing. *J. Geophys. Res.,* **101,** 12 353–12 373.
Hautala, S. L., J. L. Reid, and N. Bray, 1996: The distribution and mixing of Pacific water masses in the Indonesian Seas. *J. Geophys. Res.,* **101,** 12 375–12 389.
Hellerman, S., and M. Rosenstein, 1983: Normal monthly wind stress over the world ocean with error estimates. *J. Phys. Oceanogr.,* **13,** 1093–1104.
Hirst, A. C., and J. S. Godfrey, 1993: The role of Indonesian Throughflow in a global ocean GCM. *J. Phys. Oceanogr.,* **23,** 1057–1086.
——, and ——, 1994: The response to a sudden change in Indonesian Throughflow in a global ocean GCM. *J. Phys. Oceanogr.,* **24,** 1895–1910.
Hsiung, J., 1985: Estimates of global oceanic meridional heat transport. *J. Phys. Oceanogr.,* **15,** 1405–1413.
Kleeman, R., and S. B. Power, 1995: A simple atmospheric model of surface heat flux for use in ocean modeling studies. *J. Phys. Oceanogr.,* **25,** 92–105.
Large, W. G., J. McWilliams, and S. C. Doney, 1994: Oceanic vertical mixing: A review and a model with nonlocal boundary layer parameterization. *Rev. Geophys.,* **32,** 363–403.
Latif, M., T. Stockdale, J. Wolff, G. Burgers, E. Maier-Reimer, M. M. Junge, K. Arpe, and L. Bengtson, 1994: Climatology and variability in the ECHO coupled GCM. *Tellus,* **46A,** 351–366.
Lee, T., and J. Marotzke, 1997: Inferring meridional mass and heat transports of the Indian Ocean by fitting a general circulation model to climatological data. *J. Geophys. Res.,* **102,** 10 585–10 602.
Legler, D. M., I. M. Navon, and J. J. O'Brien, 1989: Objective analysis of pseudostress over the Indian Ocean using a direct-minimization approach. *Mon. Wea. Rev.,* **117,** 709–720.
Levitus, S., 1982: *Climatological Atlas of the World Ocean.* U.S. Govt. Printing Office, Washington, D.C., NOAA Prof. Paper No. 13. 173 pp.
——, and T. Boyer, 1994: *NOAA Atlas NESDIS 4. World Ocean Atlas 1994. Vol. 4: Temperature,* U.S. Department of Commerce. National Oceanic and Atmospheric Administration, 117 pp.
Li, Z., 1995: Intercomparison between two satellite-based products of net surface shortwave radiation. *J. Geophys. Res.,* **100,** 3221–3232.
Masumoto, Y., and T. Yamagata, 1996: Seasonal variations of the Indonesian Throughflow in a general circulation model. *J. Geophys. Res.,* **101,** 12 287–12 293.
——, and G. Meyers, 1998: Forced Rossby waves in the southern tropical Indian Ocean. *J. Geophys. Res.,* in press.
McCann, M. P., A. J. Semtner, and R. M. Chervin, 1994: Transports and heat budgets of volume, heat and salt from a global eddy-resolving ocean model. *Climate Dyn.,* **10,** 59–80.
McCreary, J. P., P. K. Kundu, and R. L. Molinari, 1993: A numerical investigation of dynamics, thermodynamics and mixed-layer processes in the Indian Ocean. *Progress in Oceanography,* Vol. 31, Pergamon Press, 181–244.
——, W. Han, D. Shankar, and S. R. Shetye, 1996: Dynamics of the East India Coastal Current. 2. Numerical solutions. *J. Geophys. Res.,* **101,** 13 993–14 010.
Mechoso, C. R., A. W. Robertson, N. Barth, M. K. Davey, P. Delecluse, P. R. Gent, S. Ineson, B. Kirtman, M. Latif, H. Le Treut, T. Nagal, J. D. Neelin, S. G. H. Philander, J. Polcher, P. S. Schopf, T. Stockdale, M. J. Suarez, L. Terray, O. Thual, and J. J. Tribbia, 1995: The seasonal cycle over the tropical Pacific in coupled ocean–atmosphere general circulation models. *Mon. Wea. Rev.,* **123,** 2825–2838.
Meyers, G., R. J. Bailey, and A. P. Worby, 1995: Geostrophic transport of Indonesian Throughflow. *Deep-Sea Res.,* **42,** 1163–1174.
Murray, S. P., and D. Arief, 1988: Throughflow into the Indian Ocean through the Lombok Strait, January 1985–January 1986. *Nature,* **333,** 444–447.
Murtugudde, R., A. J. Busalacchi, and J. Beauchamp, 1998: Seasonal-to-interannual effects of the Indonesian throughflow on the tropical Indo-Pacific Basin. *J. Geophys. Res.,* in press.
Neelin, N. D., M. Latif, M. A. F. Allaart, M. A. Cane, U. Cubasch, W. L. Gates, P. R. Gent, M. Ghil, C. Gordon, N. C. Lau, C. R. Mechoso, G. A. Meehl, J. M. Oberhuber, S. G. H. Philander, P. S. Schopf, K. R. Sperber, A. Sterl, T. Tokioka, J. Tribbia, and S. E. Zebiak, 1992: Tropical air–sea interaction in general circulation models. *Climate Dyn.,* **7,** 73–104.
Nicholls, N., 1989: Sea surface temperatures and Australian winter rainfall. *J. Climate,* **2,** 965–973.
Niiler, P. P., and E. B. Kraus, 1977: One-dimensional models of the upper ocean. *Modeling and Prediction of the Upper Layers of the Ocean,* E. B. Kraus, Ed. Pergamon Press, 143–172.
Oberhuber, J., 1988: *An Atlas Based on the 'COADS' Data Set: The Budgets of Heat, Buoyancy and Turbulent Kinetic Energy at the Surface of the Global Ocean,* p. 20, Max Planck Institute of Meteorology, Rep. No. 15.
Pacanowski, R., 1995: MOM2 documentation user's guide and reference manual. Version 1.0, GFDL Tech. Rep. 3.
——, and S. G. H. Philander, 1981: Parameterization of vertical mixing in numerical models of tropical oceans. *J. Phys. Oceanogr.,* **11,** 1443–1451.
Paulson, C. A., and J. J. Simpson, 1977: Irradiance measurements in the upper ocean. *J. Phys. Oceanogr.,* **7,** 952–956.
Perigaud, C., and P. Delecluse, 1993: Interannual sea level variations in the tropical Indian Ocean from Geosat and shallow water simulations. *J. Phys. Oceanogr.,* **23,** 1916–1934.
Peters, H., M. C. Gregg, and J. M. Toole, 1988: On the parameterization of equatorial turbulence. *J. Geophys. Res.,* **93,** 1199–1218.
Power, S. B., R. Kleeman, R. A. Colman, and B. J. McAvaney, 1995: Modeling the surface heat flux response to long-lived SST anomalies in the North Atlantic. *J. Climate,* **8,** 2161–2180.
Rahmstorf, S., and J. Willebrand, 1995: The role of temperature feedback in stabilizing the thermohaline circulation. *J. Phys. Oceanogr.,* **25,** 787–805.
Rao, R. R., R. L. Molinari, and J. F. Fiesta, 1989: Evolution of climatological near-surface thermal structure of the tropical Indian Ocean. 1. Description of mean monthly mixed layer depth, and sea surface temperature, surface currents and surface meteorological fields. *J. Geophys. Res.,* **94,** 10 801–10 815.
Reynolds, R. W., 1988: A real-time global sea surface temperature analysis. *J. Climate,* **1,** 75–86.
——, and T. M. Smith, 1994: Improved global sea surface temperature analyses using optimum interpolation. *J. Climate,* **7,** 929–948.
Schiller, A., J. S. Godfrey, P. McIntosh, and G. Meyers, 1997: A global ocean general circulation model for climate variability studies. CSIRO Rep. 227, CSIRO Division of Marine Research, Hobart, Australia, 60 pp.
——, ——, ——, and ——, 1998: Interannual dynamics and thermodynamics of the Indo-Pacific Oceans. *J. Phys. Oceanogr.,* in press.
Schmitz, W. J., 1996a: On the world ocean circulation: Vol. I. Some global features/North Atlantic Circulation, Tech. Rep. WHOI-96-03, Woods Hole Oceanographic Institution, 141 pp.
——, 1996b: On the world ocean circulation: Vol. II. The Pacific and Indian Oceans/A global update. Tech. Rep. WHOI-96-08, Woods Hole Oceanographic Institution, 237 pp.
Schneider, N., and T. Barnett, 1997: Indonesian throughflow in a coupled general circulation model. *J. Geophys. Res.,* **102,** 12 341–12 358.
Schott, F., J. C. Swallow, and M. Fieux, 1990: The Somali Current at the equator: Annual cycle of currents and transports in the upper 1000 m and connection to neighbouring latitudes. *Deep-Sea Res.,* **37,** 1825–1848.
Seager, R., and M. B. Blumenthal, 1994: Modeling tropical Pacific

sea surface temperature with satellite-derived solar radiative forcing. *J. Climate*, **7,** 1943–1957.

——, S. E. Zebiak, and M. A. Cane, 1988: A model of the tropical Pacific sea surface temperature climatology. *J. Geophys. Res.*, **93,** 1265–1280.

Simonot, J.-Y., and H. Le Treut, 1986: A climatological field of mean optical properties of the world ocean. *J. Geophys. Res.*, **91,** 6642–6646.

Sprintall, J., and M. Tomczak, 1992: Evidence of the barrier layer in the surface layer of the tropics. *J. Geophys. Res.*, **97,** 7305–7316.

Stockdale, T., D. Anderson, M. Davey, P. Delecluse, A. Kattenberg, Y. Kitamura, M. Latif, and T. Yamagata, 1993: TOGA Numerical Experimentation Group: Intercomparison of tropical ocean GCMs, World Climate Research Publication WCRP-79, WMO, Geneva, Switzerland, 43 pp.

Stricherz, J., J. O'Brien, and D. Legler, 1992: *Atlas of Florida State University Tropical Pacific Winds for TOGA 1966–1985*, Florida State University, 256 pp.

Tomczak, M., and J. S. Godfrey, 1994: *Regional Oceanography: An Introduction.* Pergamon Press, 422 pp.

Wacongne, S., and R. Pacanowski, 1996: Seasonal heat transports in a primitive equations model of the tropical Indian Ocean. *J. Phys. Oceanogr.*, **26,** 2666–2699.

Weller, R. A., and S. P. Anderson, 1996: Surface meteorology and air–sea fluxes in the western equatorial Pacific warm pool during the TOGA coupled ocean–atmosphere response experiment. *J. Climate*, **9,** 1959–1990.

Wijffels, S., N. Bray, S. Hautala, G. Meyers, and W. Morawitz, 1996: The WOCE Indonesian throughflow repeat hydrography sections: I10 and IR6. *WOCE Newsletter*, **24,** 25–28.